Dual mechanism of kinetochore microtubule detachment

William Conway[1], Gloria Ha[2], Daniel Needleman[3,4,5]
[1]Department of Physics, [2]System Biology, [3]Molecular and Cellular Biology and [4]Applied Physics, Harvard University, United States
[5]Center for Computational Biology, Flatiron Institute, United States
Correspondence: wconway@flatironinstitute.org

SUMMARY

During eukaryotic cell division, microtubules connect to chromosomes by attaching to the kinetochore via the NDC80 complex (NDC80c). The regulation of kinetochore microtubule (KMT) detachment is crucial for correcting mitotic errors. Here, we investigate the mechanism of KMT detachment by combining photoconversion measurements of KMT detachment rate, FLIM-FRET measurements of NCD80c/KMT binding, and mathematical modeling. Our results support a dual detachment mechanism in which KMTs detach from kinetochores when either 1) all NDC80c spontaneously unbind from the KMT or 2) following KMT catastrophe. We identify kinetochore components that selectively impact these two mechanisms and show that the affinity of NDC80c for KMTs is reduced at low-tension, non-bioriented kinetochores due to centromere-localized Aurora B phosphorylating the NDC80c, resulting in an elevated detachment rate for the associated KMTs. Taken together, this work leads to a biophysical model for the molecular basis of KMT detachments and their regulation during mitotic error correction.

KEYWORDS

Mitosis, kinetochore microtubule, NDC80c, MCAK, error correction

INTRODUCTION

During eukaryotic cell division, sister chromatids are connected to opposite spindle poles by microtubules bound to chromosomes at a macromolecular complex called the kinetochore (Cheeseman et al. 2008, Mussachio et al. 2017, Grishchuk et al. 2017, Joglekar et al. 2017, Monda et al. 2018, Hara et al. 2020). Erroneous kinetochore microtubule (KMT) attachments, such as when KMTs connect both sister chromatids to the same spindle pole, are thought to cause errors in chromosome segregation which can lead to aneuploidy, birth defects and cancer (Jo et al. 2001, Chaing et al. 2010, Touati and Wassmann 2016, Compton et al. 2017). To ensure accurate chromosome segregation, potential errors are actively corrected during spindle assembly. Extensive evidence suggests that this mitotic error correction process is based on selectively detaching KMTs from erroneously attached kinetochores (Cimini et al. 2001, Bakhoum et al. 2009, Godek et al. 2015, Lampson et al. 2017).

The mechanism of how KMTs detach from the kinetochore is not well understood. The NDC80c, an outer kinetochore subunit, is thought to be the primarily coupler between KMTs and the kinetochore (Cheseman et al 2006, DeLuca et al 2006, McAinsh and Marston 2022). There are approximately 200 NDC80c (Suzuki et al. 2015) and 10 KMTs (Kiewisz et al. 2022) at each kinetochore in human cells, so each KMTs can presumably interact with roughly 20 NDC80c. The NDC80c has been implicated as an important regulator of KMT stability, as have microtubule-depolymerizers such as MCAK, a kinesin-13 that localizes to centromeres during

mitosis (Hunter at al. 2003, Kline-Smith et al. 2004, Manning et al. 2007, Worderman et al. 2007, Cheeseman et al. 2008, DeLuca et al. 2011, Wimbish et al. 2021a, Kucharski et al. 2021, Tanaka et al. 2022). In addition to the NDC80c, there are many additional kinetochore subunits that interact with the KMTs, such as Ska, KNL1, MPS1, the RZZ complex, and Kif18A (Mussachio et al. 2017, Joglekar et al. 2017, Monda et al. 2018, Hara et al. 2020, Hayward et al. 2022, Mitevska et al. 2022). The relative contribution of NDC80c binding, depolymerizing kinesins, and other kinetochore subunits in regulating KMT attachments is unclear (Grischuk et al. 2017, Lampson et al. 2017, Tanaka et al 2022).

Selective detachment of KMTs from erroneously attached chromosomes is thought to be mediated by the Aurora B kinase and inter-kinetochore tension. Aurora B regulates many targets, including NDC80c, MCAK, and other kinetochore subunits, and is localized to the inner centromere during metaphase in a Haspin kinase dependent manner (Zhou et al. 2002, Lan et al. 2004, Andrews et al. 2004, Nezi et al. 2009, Akiyoshi et al. 2010, DeLuca et al. 2011, Salimian et al. 2011, Carmena et al. 2012, Godek et al. 2015, Yoo et al. 2018, Broad et al. 2020 Chen et al. 2021, McVey et al. 2021, de Regt et al. 2022). Classic experiments by Bruce Nicklas demonstrated that manually applying tension via glass microneedle decreases the KMT detachment rate; however, how Aurora B kinase activity confers tension-dependent KMT stability is not well understood (Nicklas and Koch 1969, Liu et al 2009, Posch et al. 2010, Kelly et a. 2010, Wang et al. 2010, Welburn et al. 2010, Yamagishi et al. 2010, Lampson et al. 2017, Yoo et al. 2018, Broad et al. 2020, Tanaka et al. 2022).

Here, we employ photoconversion experiments to measure the lifetime of KMTs, FLIM-FRET experiments to measure NDC80c binding to KMTs and biophysical modeling to investigate the mechanism of KMT detachment from kinetochores. We propose a dual detachment mechanism in which NDC80c binds noncooperatively to KMTs and KMTs detach from the kinetochore when either 1) all NDC80c associated with the KMT spontaneously unbind or 2) following a KMT catastrophe. This dual detachment model is consistent with the KMT lifetime and fraction of NDC80c bound to KMTs in cells with phosphomutant NDC80c as well as perturbed MCAK activity. We next developed an assay to determine whether kinetochore subunits regulated NDC80c binding or KMT catastrophe and found that Ska regulated NDC80c binding while Kif18A regulates KMT catastrophe. Finally, we investigated how KMTs are destabilized by Aurora B and low tension and found that KMT release at low tension is mediated by Haspin-recruited, centromere-localized Aurora B phosphorylation of the NDC80c, which reduces NDC80c affinity for KMTs.

RESULTS

Phosphorylation of the N-terminal tail of Hec1 regulates the lifetime of KMTs in a non-linear manner

It is well established that the NDC80c, an outer kinetochore subunit, is the primary coupler between kinetochore microtubules and chromosomes; however, little is known about how interaction with the NDC80c stabilizes the attached KMTs (Cheeseman et al. 2006, DeLuca et al. 2006, Long et al. 2017, Wimbish et al. 2020a, Warren et al 2021). To investigate this, we employed a photoconversion assay to measure the lifetime of KMTs in live human cells (DeLuca 2010; Kabeche et al. 2013). Building on previous work (Conway et al. 2022), we generated a U2OS cell line with mEOS3.2:α-tubulin to mark microtubules and SNAP-SiR:hCentrin2 to mark

the spindle poles. mEOS3.2 is a photoconvertible fluorescent protein, which switches from green to red emission after stimulation with 405nm UV light. We used a home-built photoconversion system with a 405nm diode laser to photoconvert a line of tubulin across the spindle perpendicular to the spindle axis (Wu et al. 2016, Yu et al. 2019). We then projected the photoconverted intensity onto the spindle axis (Figure 1C) and fit the profile to a Gaussian to measure the height of the peak (Figure 1D). We fit the height of the photoconverted peak, corrected for background tubulin incorporation and bleaching (Figure 1- supplement 1), to a dual-exponential decay (Figure 1E). The slow-decay lifetime of this dual exponential decay is typically attributed to the slow turnover of the stabilized KMTs, consistent with recent results from mitotic human tissue culture cells showing that the fraction of tubulin in KMTs in electron tomography reconstructions matches the slow-decay fraction of the decay after photoconversion (Conway et al. 2022). We found a mean slow-decay KMT lifetime of 4.2±0.4 minutes in wild type (WT) U2OS cells, consistent with previous measurements (Kabeche and Compton 2013).

To assess the role of the NDC80c in KMT detachment, we measured the lifetime of KMTs in cells with mutant NDC80c. The microtubule-binding face of the NDC80c is composed of two subunits: Hec1 and Nuf2 (Figure 1F upper panel). Binding between microtubules and KMTs is regulated by phosphorylation of nine sites on the N-terminal tail of the NDC80c by the Aurora kinases (Figure 1F lower panel) (Cheeseman et al. 2006, DeLuca et al. 2006, DeLuca et al. 2011, Krenn et al. 2015, Wimbish et al 2020b, Kucharski et al. 2021, Sarangapani et al. 2021). We first utilized a previously described knockdown-rescue system to generate cell lines where all nine of these residues were mutated to alanine (9A-Hec1) or aspartic acid (9D-Hec1) to mimic dephosphorylation or phosphorylation, respectively (DeLuca et al. 2011, Yoo et al. 2018). In this system, an RNAi-resistant Hec1 transgene is inserted into the genome under the control of a doxycycline inducible promoter. Endogenous Hec1 is then depleted by treatment with RNAi and replaced with mutant Hec1 by treatment with doxycycline. We found that tubulin intensity after photoconversion decayed faster in the 9D-Hec1 cells than the 9A-Hec1 cells (Figure 1G; 9D: 2.6±0.4min, 9A: 4.0±0.4min, $p = 0.014$, Student's t-test). We next investigated the effect of intermediate Hec1 N-terminal tail phosphomimetic mutants in which 1, 2, or 3 of the residues were mutated to aspartic acid while the rest were mutated to alanine (1D (S55D)-, 2D (S44,55D)-, or 3D (S15,44,55D) -Hec1) (Figure 1- supplement 2). The 1D- and 2D-Hec1 had a similar KMT lifetimes as wildtype cells, as did 9A (Figure 1H, $p=0.98$ ANOVA); however, the 3D-Hec1 mutant had a lower KMT lifetime than wildtype cells, and the lifetime of KMTs with 9D-Hec1 mutants was lower still ($p=6\times10^{-3}$ ANOVA). Since the change in KMT lifetime associated with adding an additional phosphomimicking aspartic acid differs between the mutants (i.e., 9A -> 1D and 1D -> 2D, versus 2D -> 3D), these results indicate that phosphorylation of the N-terminal tail of Hec1 regulates the stability of bound KMTs in a non-linear manner.

The free energy of NDC80-microtubule binding at kinetochores varies linearly with the number of phosphomimetic mutations

To further investigate the interaction between the KMT lifetime and Hec1 N-terminal tail phosphorylation, we next measured the fraction of NDC80c bound to KMTs using a previously developed fluorescence lifetime imaging microcopy (FLIM) – Förster resonance energy transfer (FRET) assay (Yoo et al. 2018) (Figure 2A left and center panel). Fluorescence lifetime imaging microcopy can be used to measure the fluorescence decay profile of a fluorescent molecule after

excitation with a pulsed laser. FRET occurs when donor and acceptor fluorophores with overlapping emission and excitation spectra are brought in close proximity to one another and is routinely used to measure binding between proteins (Porsch et al. 2010, Kaye et al. 2018, Algar et al. 2019, Lerner et al. 2021) If a FRET donor fluorophore has a single exponential FLIM decay curve when it is not engaged in FRET, then it will have a single exponential decay curve with a shorter mean lifetime when it engages in FRET with an acceptor fluorophore. The fraction of the donor fluorophores that engage in FRET can be measured by fitting the fluorescence decay to a dual exponential and measuring the fraction of fluorophores corresponding to the exponential with the shorter mean lifetime.

We utilized a previously generated stable U2OS cell line (Yoo et al. 2018) in which the N-terminus of the Nuf2 subunit was fused to an mTurquoise2 FRET donor and the C-terminus of β-tubulin was fused to a six amino acid residue TC tag (CCPGCC), which can bind the membrane-permeable dye FlAsH that acts as a FRET acceptor (Figure 2A, right panel). We imaged the cells with two-photon FLIM (Figure 2B) and binned the photons from kinetochores in the mTurquoise2 channel to measure the fluorescence decay of mTurquoise2 at kinetochores (Figure 2C). To characterize the fluorescence decay curves of mTurquoise2:Nuf2 at kinetochores that were not engaged in FRET, we first imaged cells expressing mTurquoise2:Nuf2 that were not stained with FlAsH. The fluorescence decay profile of the mTurquoise2 in the unstained cells profile fit well to a single exponential with a mean lifetime 3.72±0.01ns (Figure 2 – supplement 1). We next measured the fluorescence decay curves in cells stained with FlAsH and found that the fluorescence decay showed substantial deviation from a single exponential (Figure 2 – supplement 2) but was well fit to a sum of two exponentials (Figure 2C). This implies that there are two subpopulations of mTurquoise2, corresponding to two subpopulations of NDC80c, at kinetochores. The mean long lifetime of the two-exponential fit (3.69±0.03ns) was similar ($p=0.12$, Students' t-test) to the mean lifetime of the unstained cells, suggesting that the subpopulation associated with the long lifetime exponential corresponded to mTurquoise2 that was not engaged in FRET. We interpreted the fast lifetime fraction of decay curve as the fraction of mTurquoise2 engaged in FRET with TC-FlAsH because it only appeared after staining the cells with the TC-FlAsH FRET acceptor. Previously reported Monte Carlo simulations argued that mTurquoise2:Nuf2 will only engage in FRET with TC-FlAsH on the C-terminus of β-tubulin when the NDC80c is bound to KMTs, which was further supported by control experiments in which mTurquoise2 was displaced to the C-terminus of Nuf2 (Yoo et al. 2018). Based on this, we interpreted the fast lifetime fraction of decay curve as the fraction of NDC80c bound to tubulin stained with TC-FlAsH. Since only one isoform of β-tubulin was tagged with TC-FlAsH, we corrected the slow lifetime fraction by dividing by the fraction of tubulin stained with TC-FlAsH to determine the fraction of NDC80c bound to KMTs as described previously (Yoo et al. 2018). To avoid bias in the exponential fitting, we used a previously reported Bayesian fitting algorithm (Kaye et al. 2017) where we fixed the long lifetime to the mean mTurquoise2 lifetime in unstained cells in our final analysis. Using this procedure, we found that the mean fraction of NDC80c bound to KMTs in wild type metaphase spindles was 0.28±0.02.

To determine how phosphorylation of the Hec1 N-terminal tail affects binding between KMTs and the NDC80c, we next measured the fraction of NDC80c bound to KMTs in cells expressing phosphomutant Hec1 using the FLIM-FRET assay. To do so, we inserted a phosphomutant Hec1 transgene under the control of a doxycycline inducible promoter into the genome of the mTurquoise2:Nuf2 and β-tubulin:TC-FlAsH cell line we used in our FLIM-FRET assay and employed the knockdown-rescue protocol described above to replace endogenous

Hec1 with phosphomutant Hec1. We first explored how the number of phosphorylated residues impacted NDC80c-KMT binding by comparing the fraction of NDC80c bound in 9A-, 1D-, 2D-, 3D- and 9D-Hec1 mutants. We found that increasing the number of phosphorylated residues decreased the NDC80c fraction bound ($p=2.2\times10^{-14}$ ANOVA) (Figure 2E). We then probed how the position of the phosphorylated residues in 1D-Hec1 cells, which had similar NDC80c bound fractions as wild type cells (p= 0.97 ANOVA), impacted the interaction between KMTs and the NDC80c. We found that the fraction of bound NDC80c was the same (p=0.94 ANOVA) in five 1D-Hec1 mutant cell lines which only differed in the position of a single D residue, indicating that the position of phosphorylated residue does not significantly impact NDC80c-KMT binding (Figure 2D). Taken together, these results demonstrate that the number, not the position, of phosphorylated Hec1 N-terminal tail sites regulates NDC80c-KMT binding.

We next sought to interpret our results using a previously constructed two-state model of NDC80c binding to KMTs (Yoo et al. 2018) in which bound NDC80c unbinds from KMTs at rate k_{off} and unbound NDC80c binds to KMTs at rate k_{on}, resulting in a steady-state fraction of NDC80c bound to KMTs of $f_{bound} = \frac{k_{on}}{k_{on}+k_{off}}$. In this model, the fraction of NDC80c bound to KMTs is related to the free energy difference between the bound and unbound state, following the general relationship which holds for such two-state models (Silbey et al 2005):

$$\Delta G^0 = k_B T \ln \frac{k_{on}}{k_{off}} = k_B T \ln \frac{f_{bound}}{1-f_{bound}} \quad (1).$$

Thus, the free energy difference between bound and unbound NDC80c can be determined from f_{bound}, which we experimentally measured with FLIM-FRET. We calculated the free energy difference between the bound and unbound NDC80c for the 9A-, 1D-, 2D-, 3D-Hec1 phosphomutants and found that each additional phosphorylated residue linearly increased the free energy difference by $\Delta G^0/Site$=0.42 ± 0.02k_BT (Figure 2F). Prior *in-vitro* measurement of individual NDC80c binding to MTs found that each phosphorylated residue increased the free energy difference of a single NDC80c binding to MTs by a similar, but slightly lower, amount, $\Delta G^0/Site$ =0.30 ± 0.02k_BT ($p=5\times10^{-7}$ Bayesian model comparison) (Zaystev et al. 2015). To investigate whether the NDC80c bound cooperativity to the KMTs, we fit the experimentally measured free energy differences to a model which included a cooperative term in the free energy (Figure 2F, see *Methods)*. We found that the NDC80c-NDC80c interaction energy J=0.0 ± 0.1k_BT was much weaker than the binding energy of NDC80c to KMTs and was not statistically distinguishable from a model with no cooperativity (p=0.99 Bayesian model comparison). This argues that NDC80c-KMT binding at kinetochores is not cooperative, consistent with prior *in-vitro* single molecule experiments of free NDC80c binding to KMTs (Zaystev et al. 2015). Thus, these FLIM-FRET results indicate that the number, not the position, of phosphorylated Hec1 N-terminal tail residues regulates the binding between ND80c and KMTs, and that NDC80c at kinetochores bind uncooperatively to KMTs.

KMTs detach when all the NDC80c spontaneously unbind or following KMT catastrophe

To investigate the mechanism of how KMTs detach from the kinetochore, we next developed a biophysical model to connect the NDC80c bound fractions observed in the FLIM-FRET experiments to the KMT lifetimes observed in the photoconversion experiments. We consider models in which there are a fixed number, N, of NDC80s per KMT, each of which is

either bound or unbound to the KMT, and in which the KMT detaches from the kinetochore when no NDC80cs are bound to it (Figure 3A). Our Hec1 phosphomutant photoconversion and FLIM-FRET experiments indicated that perturbing NDC80c binding kinetics altered the KMT lifetime, so we initially explored a model where only NDC80c binding kinetics regulated the KMT lifetime. Motivated by our FLIM-FRET results that NDC80c binding to KMTs was not cooperative, we assumed that NDC80cs independently bind and unbind to KMTs (Figure 3B, left), thus the transition rate from a state with n_i NDC80c bound to a state with n_{i-1} NDC80c bound is given by the rate that any of n_i bound NDC80c unbind from the KMT, $n_i k_{off}$, and the n_{i-1} state transitions to the n_i state at the rate that any of the $(N - n_{i-1})$ unbound NDC80c bind to the KMT, $(N - n_{i-1})k_{on}$ (Figure 3B, center). In this model, a KMT detaches from the kinetochore after that last NDC80s unbinds it.

To determine whether this model, in which KMT detachment is determined solely by NDC80c binding kinetics, was consistent with both the NDC80c bound fraction and KMT lifetime experiments, we calculated the predicted KMT lifetime as a function of NDC80c bound fraction and compared the model-prediction to the Hec1 phosphomutant experiments. To do so, we computed the mean first passage time from the steady state distribution to the no NDC80c bound, detached KMT state as a function of the NDC80c bound fraction using the fundamental matrix method (Allen 2010, see *Methods*). This model has three parameters: N, k_{off}, and k_{on}. Based on prior measurements of the number of NDC80c (~200 NDC80c/kinetochore - Suzuki et al. 2015) and the number of KMTs (~10 KMTs/kinetochore - Kiewisz et al. 2022) at each kinetochore, we set $N = 20$ NDC80c per KMT. Under the reasonable assumption that Hec1 phosphorylation acts by changing the free energy of the bound state, k_{off} will vary between phosphomutants while k_{on} will remain constant. Since k_{off} is related to k_{on} by $k_{off} = \frac{1-f_{bound}}{f_{bound}} k_{on}$, and f_{bound} is experimentally measured for the phosphomutants, there is only a single unknown parameter in the model to be fit to the phosphomutant data, k_{on}. A best fit to this model predicts a sharp increase in KMT lifetime with increasing f_{bound}, in clear disagreement with experimental measurements (Figure 3B, right). A model where all NDC80c bind cooperatively as a single binding unit predicts a similar increase in the KMT lifetime with increasing fraction bound indicating that the disagreement between and NDC80c binding alone model is not a consequence of assuming independent NDC80c binding (Figure 3 – supplement 2). Thus, a model in which KMTs detach only when all NDC80c unbind is not consistent with the observed KMT lifetime and NDC80c fraction bound in the Hec1 phosphomutants.

Prior work has demonstrated that both NDC80c phosphorylation (DeLuca et al. 2006, Zaystev et al. 2015, Yoo et al. 2018, Wimbish et al. 2020a) and the activity of microtubule catastrophe factors (Lan et a. 2004, Andrews et al. 2004, Worderman et al 2007, Manning et al. 2007, Godek et al. 2014, Warren et al. 2022) can regulate the lifetime of KMTs. We therefore sought to incorporate the impact of catastrophe factors into a model of KMT detachment. We proposed that, in addition to KMTs detaching due to NDC80c unbinding, KMTs can also catastrophically detach at a constant rate k_{cat} that is independent of NDC80 binding (Figure 3C, center panel). In this model, the KMT can detach when either all NDC80c spontaneously unbind from the KMT or after the KMT undergoes a catastrophe. We then calculated the KMT lifetimes predicted by this model and found that the model predictions fit well to the Hec1 phosphomutant data (k_{on}=0.096±0.004min^{-1} and k_{cat}=0.25±0.01min^{-1}) (Figure 3C, right). We conclude that a dual-detachment model, where KMTs detach when either all the NDC80c unbind from the KMT

or following catastrophic detachment, is consistent with both the KMT lifetime and the NDC80c binding observed in the Hec1 phosphomutants.

To further test this proposed dual-detachment model, we investigated the impact of perturbing MCAK, a known catastrophe factor (Hunter at al. 2003, Manning et al. 2007, Wonderman et al. 2007, Godek et al, 2015, McHugh 2019, Tanaka 2022). We used the knockdown-rescue protocol to investigate cells with WT Hec1 and 9A, 2D, and 9D Hec1 phosphomutants that were either subject to MCAK RNAi knockdown or treated with UMK57, a small molecule MCAK potentiator (Wordermann et al. 1995, Hunter at al. 2003, Kline-Smith et al. 2004, Wordermann et al. 2007, Manning et al. 2007, Domnitz et al. 2012, Orr et al. 2016) (Figure 4A). We performed FLIM-FRET under these different conditions to measure the impact on NDC80c binding (Figure 4B) and photoconversion to measure KMT lifetimes (Figure 4C). We combined these two datasets by plotting KMT lifetime vs NDC80c bound fraction and fit the resulting curve with the predictions from the dual-detachment model (Figure 4D). Both the MCAK RNAi and UMK57 data fit well to the dual detachment model, with the same NDC80c parameters as control cells, but a lower KMT catastrophe rate than wildtype (k_{cat}=0.19±0.02min^{-1}, p=0.02 Bayesian parameter comparison) in the MCAK RNAi cells and a higher KMT catastrophe rate than wildtype in the UMK57 cells (k_{cat}=0.34±0.02min^{-1}, p=3x10^{-4} Bayesian parameter comparison). Thus, hyperactivating MCAK with UMK57 increases the catastrophe rate and inhibiting MCAK activity by RNAi knockdown decreases the catastrophe rate, both without modifying NDC80c-KMT interactions (Figure 4E). This behavior is consistent with prior work demonstrating that MCAK is a catastrophe factor that can modulate KMT stability (Hunter at al. 2003, Manning et al. 2007, Wonderman et al. 2007, Godek et al, 2015, Domnitz et al. 2012, Orr et al. 2016, McHugh 2019, Tanaka 2022), and further supports the validity of the dual-detachment model in which KMTs detach from the kinetochore due to either: 1) all NDC80cs spontaneously unbinding or 2) catastrophic detachment.

Kif18a is a KMT catastrophe factor; Ska regulates NDC80c binding via Hec1 N-terminal tail phosphorylation

Metazoan kinetochores are composed of more than 80 different subunits and associated proteins in addition to the NDC80c that connect KMTs to chromosomes and regulate KMT attachment (Cheeseman and Desai 2008, Joglekar et al. 2017, Mussachio et al. 2017, Monda et al, 2018, Hara et al. 2020). The role of many of these factors in regulating KMT attachment is not well understood. In the dual detachment model, the KMT detachment rate can be regulated in two ways: 1) By altering NDC80c binding to KMTs (i.e., k_{off}) or 2) By altering the KMT catastrophe rate (i.e., k_{cat}). The predictions of the dual-detachment model suggest a means of determining which of these two pathways is regulated by a given factor: First, measure the KMT lifetime and the NDC80c bound fraction in cells where the factor has been inhibited and compare the measurements to WT cells (Figure 5A). If the factor only affects NDC80c binding to KMTs, via the k_{off} unbinding rate, then the data from the inhibited cells will lie on the same model curve as the WT data. If the factor instead affects the KMT catastrophe rate k_{cat}, then the data from the inhibited cells will lie off the original model fit curve and instead along a curve with a different catastrophe rate. Next, measure KMT lifetime and NDC80c fraction bound in Hec1 phosphomutant cells where the factor has been inhibited and fit the resulting curves using the dual-detachment model, thereby measuring k_{cat} (Figure 5B). Taken together, this approach

provides a means to determine how given factors influence both NDC80c binding to KMTs and the KMT catastrophe rate.

We first used this approach to investigate the role of Kif18A, a kinesin-8 that regulates KMT detachments and is required for proliferation in many cancer cell lines, though not required for proliferation in many non-cancerous cell lines (Stumpff et al. 2008, Manning et al. 2010, Edzuka et al. 2018, Edson et al. 2022). We knocked down Kif18A with RNAi and performed photoconversion experiments, which revealed that the KMT lifetime was lower in Kif18A knockdown cells (p=0.01, Students' t-test), and FLIM-FRET experiments, which revealed that the NDC80c fraction bound was statistically indistinguishable from control cells (p=0.11 Students' t-test) (Figure 5C,D). This suggests that Kif18A regulates KMT detachments by modifying the KMT catastrophe rate, not NDC80c binding. To study this in more detail, we measured KMT lifetime and NDC80c binding in Kif18A RNAi knockdown cells expressing 9A-Hec1. Fitting the data from Kif18A RNAi in both WT and 9A-Hec1 cells using the dual-detachment model gave k_{cat}= 0.34±0.03min^{-1}, confirming that Kif18A knockdown alters the KMT catastrophe rate (p=4x10^{-6} Bayesian model comparison) (Figure 5E). We therefore conclude that Kif18A alters KMT stability through its activity as a catastrophe factor and does not affect NDC80c binding.

We next investigated the role of Ska, a microtubule binding kinetochore subunit that localizes to the outer kinetochore (Hanisch et al. 2006, Raajimakers et al. 2009, Theis et al. 2009). It has been proposed that Ska alters KMT stability either by crosslinking NDC80cs (Gaitanos et al. 2009, Welburn et al. 2009, Abad et al. 2014, Jacynk et al. 2017, Wimbish et al. 2020b) or by recruiting Aurora B and PP1 to the kinetochore (Rendli et al. 2016, Sivakumar et al. 2016). We knocked down the Ska3 subunit with RNAi and performed photoconversion experiments and FLIM-FRET experiments, which revealed that the NDC80c bound fraction was lower in the Sk3a RNAi knockdown cells (p=0.01, Students' t-test) and the KMT lifetime decreased (but with only marginal statistical significance, p=0.1, Students' t-test) (Figure 5F,G). The data for the Ska3 RNAi knockdown cells still lay on the WT dual detachment model curve (p=0.45 Bayesian model comparison), suggesting that Ska modulates NDC80c binding to KMTs. We next measured KMT lifetime and NDC80c binding in Ska3 RNAi knockdown cells expressing 9A-Hec1. Fitting the data from Ska3 RNAi in both WT and 9A-Hec1 cells using the dual-detachment model gave k_{cat} = 0.25±0.03min^{-1}, a KMT catastrophe rate that is statistically indistinguishable from controls (p=0.97, Bayesian model comparison) (Figure 5H), indicating that Ska does not modulate KMT catastrophes. The 9A-Hec1 Ska3 RNAi cells have very similar NDC80c bound fractions and KMT lifetimes to 9A-Hec1 cells without Ska3 knockdown (NDC80c bound fraction: p=0.87, Students' t-test; KMT lifetime: p=0.56, Students' t-test), arguing that Ska-based regulation of NDC80c binding occurs via Hec1 tail phosphorylation.

Haspin-localized Aurora B destabilizes low-tension KMTs by regulating NDC80c binding

Aurora B kinase plays a key role in mitotic error correction and in regulating KMT detachments (Yoo et al. 2018, Tanaka et al. 2022, Barbosa et al. 2022) (Figure 6). Aurora B phosphorylates many targets, including both MCAK and the N-terminal tail of Hec1 in the NDC80c (Tanaka et al. 2002, Lan et al. 2004, DeLuca et al. 2006, Tauchmann et al. 2015, Krenn et al. 2015, Broad et al. 2020). In metaphase, Aurora B localizes to inner-centromeres in a Haspin kinase dependent manner, and it has previously been shown that the Haspin inhibitor 5-iodotubercidin (5-ITu) prevents recruitment of Aurora B to centromeres (Wang et al. 2010,

Kelley et al. 2010, Yamagishi et al. 2010, Carmena et al. 2012, Barbosa et al. 2022, Wang, et al. 2012, Yoo et al. 2018). We next explored the extent to which, and in what manner, Aurora B regulates KMT catastrophes and NDC80c binding to KMTs.

We first inhibited Aurora B with the drug ZM447439 (Ditchfield et al. 2003) and performed both photoconversion experiments and FLIM-FRET experiments. The KMT lifetime significantly increased after Aurora B inhibition (p=0.03, Students' t-test) resulting in the Aurora B inhibited point falling off the dual-detachment model curve of WT cells and indicating that inhibiting Aurora B altered the KMT catastrophe rate (Figure 6B). The increase in the NDC80c fraction bound after Aurora B inhibition was not statistically significant (p=0.3, Students' t-test), which is surprising because Aurora-B is known to phosphorylate NDC80c (DeLuca et al. 2006, Cheeseman et al. 2006, Krenn et a. 2015, Zaystev et al. 2016, Yoo et al. 2018, McVey et al. 2021). We speculate the explanation for the lack of impact of Aurora-B inhibition on NDC80c binding in metaphase is because, at this time in mitosis, the wild type NDC80c bound fraction is similar to the almost fully de-phosphorylated 1D-Hec1 mutant (p=0.97; ANOVA), so Aurora B inhibition likely does little to alter the bound fraction of the already mostly de-phosphorylated wild type metaphase NDC80c. Consistent with this hypothesis, previous work showed that inhibiting Aurora-B in prometaphase, when NDC80c binding is lower than in metaphase, does lead to a significant increase in NDC80c binding (Yoo et al. 2018). We next performed photoconversion and FLIM-FRET measurements on ZM447439 treated, Hec1 phosphomutant cells and fit the dual detachment model, giving k_{cat} = 0.16±0.02min^{-1} (Figure 6C), which is significantly less than the catastrophe rate in WT cells (p=2x10^{-3} Bayesian model comparison). Thus, global inhibition of Aurora B in metaphase primarily stabilizes KMT detachments by reducing catastrophes. To explore the role of the centromere localized Aurora B pool, we next disrupted Aurora B localization to centromeres with 5-ITu (Wang et al. 2009, Wang, et al. 2012, Yoo et al. 2018) and performed photoconversion experiments and FLIM-FRET experiments. The 5-ITu data remained on the dual-detachment model curve of WT cells (Figure 6D). We took photoconversion and FLIM-FRET measurements of 5-ITu treated, Hec1 phosphomutant cells and fit the dual detachment model, giving k_{cat}=0.24±0.02min^{-1}, which is indistinguishable from the catastrophe rate in WT cells (p=0.81, Bayesian model comparison) (Figure 6E). Taken together, this indicates that Aurora B regulates both KMT catastrophes and NDC80c binding to KMTs, but the pool of Aurora B recruited to centromeres by Haspin only regulates NDC80c binding.

In classic experiments, Bruce Nicklas showed that applying tenson to kinetochores with a glass needle reduces the KMT detachment rate (Nicklas and Koch, 1969). The decreased stability of KMTs subject to low tenson relative to those at high tension is believed to be crucial for mitotic error correction (Nicklas and Koch 1969, Nicklas 1995, Akiyosh et al. 2010, Welburn et al. 2010, Salimian et al. 2011, McVey et al. 2021). It has been proposed that the tension dependency of KMT detachments results from Aurora B activity, but the precise manner by which this occurs remains unclear (Bakhoum et al. 2009, Liu et al. 2010, Salimian et al. 2011, Zaystev et al. 2015, Godek et al. 2015, Yoo et al. 2018, Chen et al. 2021; Wang et al. 2011, Lampson et al. 2017, de Regt et al. 2022). To investigate this further, we performed experiments in monopolar spindles, generated by inhibiting kinesin-5 with a small molecule inhibitor, monastrol, where it has been previously shown that kinetochores are under low tension (Kapoor et al 2001, Maliga et al. 2002, Yoo et al. 2018, Chen et al. 2021). We measured the KMT lifetime and fraction of NDC80c bound to KMTs in the low tension, monopolar spindles and found that both the KMT lifetime (p=8x10^{-4} Students' t-test) and fraction of NDC80c bound

($p=2x10^{-3}$ Students' t-test) were lower in monopolar spindles than WT bipolar spindles, but the monopolar spindle datapoint still lay on the same fit dual-detachment model curve as WT bipolar spindles (Figure 6F). This suggests that the low tension KMTs are destabilized by weakened NDC80c binding to KMTs. We measured the KMT lifetime and NDC80c bound fraction in monopolar spindles expressing a 9A-Hec1 phosphomutant and found that they had the same NDC80c bound fraction and KMT lifetime as biopolar 9A-Hec1 spindles (NDC80 bound fraction: p=0.60, Students' t-test; KMT lifetime: p=0.61, Students' t-test), arguing that the tension dependency of KMT detachments requires the phosphorylation of the Hec1 N-terminal tail. Combining the data from monopolar spindles with WT Hec1 and monopolar spindle with Hec1 phosphomutants and fitting to the dual-detachment model gave a KMT catastrophe rate of k_{cat} = 0.27±0.01min^{-1} in monopolar spindles, statistically indistinguishable from the KMT catastrophe rate in bipolar spindles (p=0.85, Bayesian model comparison) (Figure 6G). Taken together, these results indicate that low tension KMT detachments are destabilized due to phosphorylation of the Hec1 tail reducing the affinity of NDC80c to KMTs (without modulation of KMT catastrophes). We next investigated the contribution of centromere localized Aurora B to destabilizing low tension KMT detachments by treating monopolar spindles with the 5-ITu Haspin inhibitor. We performed photoconversion experiments and FLIM-FRET experiments, which revealed that the addition of 5-ITu to monopoles caused an increase in both NDC80c fraction bound and KMT lifetimes relative to monopoles without 5-ITu (NDC80 bound fraction: p=0.02, Students' t-test; KMT lifetime: p=0.02, Students' t-test), to values which were indistinguishable to those of WT bipolar spindles (NDC80 bound fraction: p=0.31 Students' t-test; KMT lifetime: p=0.65, Students' t-test) (Figure 6H). This indicates that centromere-localized Aurora B is required for destabilizing KMTs at low tension.

DISCUSSION

The removal of incorrectly attached KMTs is crucial for the correction of mitotic errors and proper chromosome segregation; however, the mechanism by which KMTs detach from the kinetochore, and how KMTs are selectively destabilized at erroneously attached chromosomes, is not well understood. Our results support a dual-detachment mechanism where individual NDC80c independently bind and unbind to KMTs and KMTs detach either when all the associated NDC80c spontaneously unbind or following a KMT catastrophe. In this model, KMT stability can be regulated by altering either the rate that NDC80c unbind from KMTs or the KMT catastrophe rate. We investigated whether perturbing factors known to regulate KMT attachment to the kinetochore altered either NDC80c binding or KMT catastrophes and found that Ska regulates NDC80c binding and Kif18A regulates KMT catastrophes. We found that the Aurora B kinase regulated both NDC80c binding and KMT catastrophes, though disrupting Aurora B localization to the inner centromere by inhibiting the Haspin kinase only impacted NDC80c binding. To investigate how KMTs are selectively destabilized at erroneously attached chromosomes, we performed experiments in monopolar spindles where chromosomes are erroneously attached and subject to low tension. We found that NDC80c binding was perturbed in monopolar spindles, but the KMT catastrophe rate was similar to wild-type bipolar metaphase spindles. Disrupting Aurora B localization to inner centromeres by inhibiting Haspin kinase with 5-ITu restored the NDC80c binding and KMT stability of monopolar spindles to the levels they exhibit in wild-type bipolar metaphase spindles. Taken together, these results support a model in

which KMTs at erroneously attached chromosomes are destabilized by Haspin-localized Aurora B kinase phosphorylating Hec1 and thereby regulating NDC80c binding to KMTs.

The dual-detachment mechanism provides insights into the biophysics of the interaction between the NDC80c and KMTs (Figure 7A, left). We found that free energy difference associated with NDC80c binding and unbinding to KMTs increased linearly with each successive phosphorylation of the Hec1 N-terminal tail (Figure 2). Consistent with prior *in-vitro* single molecule experiments (Zaystev et al. 2015), the fit interaction energy between bound NDC80cs was much weaker than the binding energy of NDC80s with KMTs, indicating that binding between NDC80c and KMTs at kinetochores was not cooperative. Our tubulin photoconversion measurements indicate that KMTs remain attached to the kinetochore for an average of 4.2 ± 0.4 min. The fit NDC80c unbinding rate in the dual-detachment model was 0.26 ± 0.4 min^{-1}, meaning that an NDC80c remains bound to a KMT for of 3.9 ± 0.7 min. Tubulin dimers incorporate at the plus end of KMTs and flux away from the kinetochore along the walls of the KMTs by subsequent tubulin polymerization at the plus end at a rate of ~1 μm/min (Kabeche and Compton 2013, Stebylyanko et al. 2020, Conway et al 2022), so over the ~4 minutes that an NDC80c remains bound to the kinetochore, a tubulin dimer will move ~4 μm from the kinetochore. Since the NDC80c remain localized at the kinetochore, the NDC80c must transition from binding one tubulin dimer to another tubulin dimer to remain bound to the KMT, perhaps diffusing along the surface of the microtubule as proposed in prior work (Powers et al. 2009, Schwietert et al. 2022).

The regulation of KMT stability is crucially important for ensuring accurate chromosome segregation (Cimini et al. 2001, Bakhoum et al. 2009, Godek et al. 2015, Lampson et al. 2017). We investigated how several factors proposed to regulate KMT stability function in the context of the dual detachment model, where KMTs can be destabilized by either increasing the rate that NDC80c unbind from KMTs or by increasing the KMT catastrophe rate (Figure 7A, right). We examined the Ska complex, a kinetochore subunit whose role in regulating KMT attachments is not well understood (Daum et al. 2009, Gaitanos et al. 2009, Theis et al. 2009, Abad et al. 2014). Prior work has proposed Ska may link NDC80c together cooperatively to enable load bearing at kinetochores (Welburn et al. 2009, Schmidt et al. 2012, Janzyck et al. 2017, Aukland et al. 2017) and/or may recruit kinase and phosphatases to regulate NDC80c phosphorylation (Rendli et al. 2016, Sivakumar et al. 2016). By fitting data from Ska knockdown cells to the dual-detachment model, we found that Ska regulated NDC80c biding to KMTs, but not KMT catastrophes (Figure 5). Knocking down Ska decreased the fraction of NDC80c bound to KMTs in WT-Hec1 cells but did not alter the fraction of NDC80c bound or the KMT lifetime in de-phosphomimetic 9A-Hec1 cells, implying that NDC80c phosphorylation is required for Ska to regulate NDC80c binding. This is consistent with the hypothesis that Ska recruits kinases/phosphatases that regulate NDC80c phosphorylation to the kinetochore. Furthermore, our analysis of the free energy change associated with NDC80c phosphorylation (Figure 2) suggested that NDC80c bind uncooperatively to KMTs, which is inconsistent with the hypothesis that Ska links many KMTs together to bind cooperatively. Taken together, our results indicate that Ska regulates KMT stability by modulating NDC80c binding, likely by recruiting factors that (de-)phosphorylate the NDC80c.

We next investigated the role of Kif18A, a kinesin-8 that localizes to kinetochores during metaphase (Mayr et al. 2007, Stumpff et al. 2008), whose role in regulating KMT attachments is not well understood. Prior work has proposed that Kif18A plays an important role in chromosome congression (Malaby et al. 2019, Marquis et al. 2021) and may depolymerize

KMTs (Mayr et al. 2007) and/or suppress plus-end microtubule dynamics (Stumpff et al. 2008). By fitting data from Kif18A knockdown cells to the dual detachment model, we found that Kif18A regulated the KMT catastrophe rate (Figure 5). Expressing 9A-Hec1 phosphomutants did not restore the wild-type KMT lifetime in Kif18A knockdown cells, further arguing that Kif18A did not regulate KMT attachment via NDC80c binding. This indicates that Kif18A regulates KMT stability by decreasing the KMT catastrophe rate. Regulatory factors can therefore modulate KMT stability by regulating either the NDC80c binding detachment mechanism (e.g., Ska) or the KMT catastrophe detachment mechanism (e.g., Kif18A).

We then investigated the role of the Aurora B kinase, a key mitotic regulatory kinase (Liu et al 2009, Posch et al. 2010, Kelly et a. 2010, Wang et al. 2010, Welburn et al. 2010, Yamagishi et al. 2010, Lampson et al. 2017, Yoo et al. 2018, Broad et al. 2020, Tanaka et al. 2022) that is recruited to centromeres by the Haspin kinase and has many targets including NDC80c (Cheeseman et al. 2006, DeLuca et al. 2006), Ska (Redli et al. 2016) and MCAK (Andrews et al. 2004). By fitting data from cells treated with an Aurora B inhibitor, ZM447439, to the dual detachment model, we found that inhibiting Aurora B lowered the KMT catastrophe rate (Figure 6). Cells expressing NDC80c mutants mimicking Aurora B phosphorylation showed different affinity between NDC80c and KMTs (Figure 2). Based on these results, we propose that Aurora B regulates KMT stability by regulating both NDC80c binding and KMT catastrophes (Figure 7B). Aurora B can regulate NDC80c directly by phosphorylating NDC80c; however, Ska, which we argue regulates NDC80c binding by recruiting kinases/phosphatases, is also an Aurora B target (Redli et al. 2016), so Aurora B can also regulate NDC80c indirectly by phosphorylating factors that themselves regulate NDC80c. Aurora B is not known to directly interact with tubulin, so it must regulate KMT catastrophes by phosphorylating factors that regulate KMT catastrophes such as MCAK, which is, indeed known to be regulated by Aurora B phosphorylation (Andrews et al. 2004, Zhang et al. 2007, Ems-McClung et al. 2013, Shao et al. 2015). Taken together, our results lead us to conclude that Aurora B regulates KMT stability by impacting both detachment mechanisms (Figure 7A): 1) Aurora B regulates NDC80c phosphorylation both directly by phosphorylating it and indirectly via Ska (and possibly other factors) and 2) Aurora B regulates KMT catastrophes via MCAK (and possibly other factors). A similar experimental approach could be used to dissect how other factors impact KMT stability.

Selective stabilization of KMTs attached to bioriented chromosomes is crucial to ensure accurate chromosome segregation and is thought to be mediated by the Aurora B kinase and an increase in inter-kinetochore tension upon biorientation. Classic experiments by Bruce Nicklas demonstrated that manually applying tension across kinetochores with a microneedle stabilizes KMTs, implying that increased inter-kinetochore tension at bioriented kinetochores selectively stabilizes KMTs attached to bioriented chromosomes (Nicklas and Koch 1969). Consistent with both Nicklas' microneedle experiment and prior photoconversion experiments (Kabeche and Compton 2013), we found that the KMT lifetime was lower in monopolar spindles, where chromosomes cannot biorient and kinetochores are at low tension (Wang et al. 2010, Kelley et al. 2010, Yamagishi et al. 2010, Carmena et al. 2012, Wang, et al. 2012, Yoo et al. 2018, Barbosa et al. 2022). The mechanism of how increased inter-kinetochore tension confers stability to KMTs, is not well understood, though the higher concentration of Aurora B kinase at low-tension kinetochores than at high-tension kinetochores is thought to be crucial for conferring tension-dependent KMT stabilization (Zhou et al. 2002, Lan et al. 2004, Andrews et al. 2004, Nezi et al. 2009, Akiyoshi et al. 2010, DeLuca et al. 2011, Salimian et al. 2011, Carmena et al. 2012, Godek et al. 2015, Broad et al. 2020 Chen et al. 2021, McVey et al. 2021, de Regt et al. 2022). By

fitting the monopolar spindle data to the dual detachment model, we found that NDC80c binding to KMTs was weaker in monopolar spindles than in bipolar spindles, but the KMT catastrophe rate was similar (Figure 6), indicating that tension dependent KMT stabilization is mediated by regulating NDC80c binding. Inhibiting Aurora B phosphorylation of the NDC80c, either by expressing 9A-Hec1 phosphomutants that Aurora B cannot phosphorylate or by decreasing the concentration of Aurora B at kinetochores by inhibiting the Haspin kinase, prevented KMT lifetime and NDC80c binding from decreasing in monopolar spindles (relative to bipolar spindles), indicating that tension-dependent regulation of NDC80c binding is mediated by Aurora B phosphorylation of NDC80c. Taken together, these observations are consistent with a model for destabilizing erroneous, low tension KMT attachments based on phosphoregulation of NDC80c-KMT binding by Aurora B: the concentration of Aurora B at kinetochores is regulated by tension in a Haspin dependent manner, such that low-tension kinetochores are associated with higher concentrations of Aurora B, which leads to more NDC80c phosphorylation, weaker NDC80c binding to KMTs and destabilized KMTs (Figure 7B). Further testing this proposal will require careful quantification of the mitotic error rate in response to perturbed KMT lifetime and perturbed Aurora B activity, which will be an exciting challenge for future experiments. This would extend the model we propose here from the molecular interaction of the NDC80c with KMTs and the regulation of KMT attachment to the correction of mitotic errors and accurate chromosome segregation.

AUTHOR CONTRIBUTIONS

Conceptualization, W.C. and D.J.N.; Methodology, W.C. and D.J.N.; Investigation, W.C. and G.H.; Writing – Original Draft, W.C. and D.J.N.; Writing – Review & Editing, W.C. and D.J.N.; Funding Acquisition, D.J.N.; Supervision, D.J.N.

ACKNOWLEDGEMENTS

This work was supported by the NSF-Simons Center for Mathematical and Statistical Analysis of Biology at Harvard (award number #1764269) and the Harvard Quantitative Biology Initiative. W. Conway was supported by National Science Foundation GRFP Fellowship # 2018238646.

DECLARTION OF INTERESTS

The authors declare no competing interests

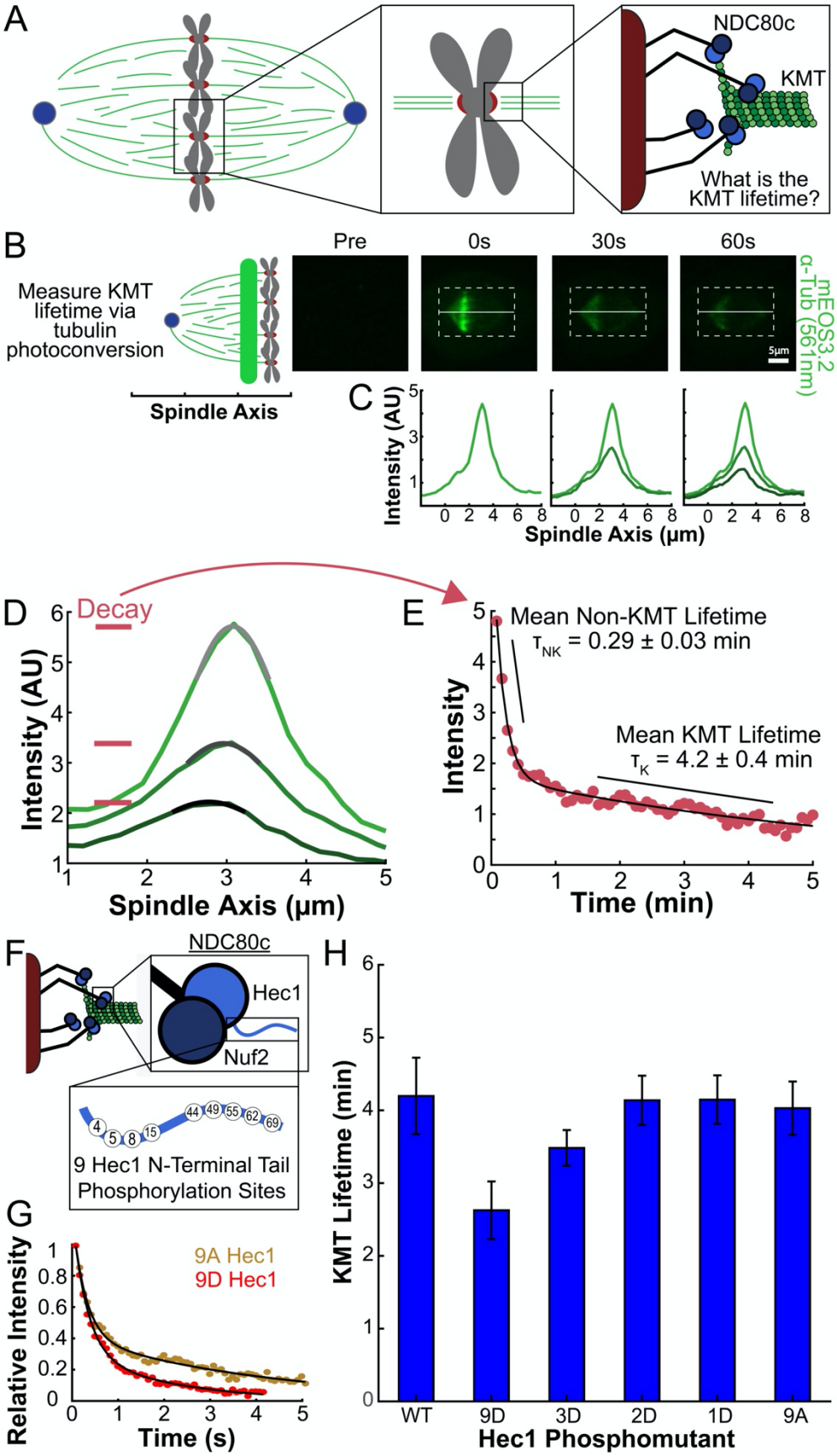
A
NDC80c
KMT
What is the KMT lifetime?
B
Measure KMT lifetime via tubulin photoconversion
Spindle Axis
Pre
0s
30s
60s
5μm
mEOS3.2 α-Tub (561nm)
C
Intensity (AU)
Spindle Axis (μm)
D
Decay
Intensity (AU)
Spindle Axis (μm)
E
Mean Non-KMT Lifetime
τ_{NK} = 0.29 ± 0.03 min
Mean KMT Lifetime
τ_K = 4.2 ± 0.4 min
Intensity
Time (min)
F
NDC80c
Hec1
Nuf2
9 Hec1 N-Terminal Tail Phosphorylation Sites
G
9A Hec1
9D Hec1
Relative Intensity
Time (s)
H
KMT Lifetime (min)
WT
9D
3D
2D
1D
9A
Hec1 Phosphomutant

Figure 1: Photoconversion measurements of KMT stability A) The metaphase spindle (left) with a zoom-in on a single chromosome depicting microtubules bound to the opposite sister kinetochores (center) and NDC80c bound to a single KMT (right). B) Images from a photoconversion experiment showing SNAP:centrin (magenta) and mEOS3.2:α-tubulin (green). Images are shown immediately preceding, 0, 30, and 60s after photoconversion with a focused 405nm diode laser C) Line profile generated by averaging 3.5μm on either side of the spindle axis in dotted box in B. D) Line profiles (shades of green) fit to Gaussian profiles (shades of gray). Lighter shades are earlier times. E) Red dots: Fit intensity of the line profile over time, corrected for background and bleaching. Black line: dual-exponential fit decay. F) NDC80c bound to KMTs (top left). The Hec1 and Nuf2 subunits (middle) bind to KMTs. NDC80c binding is regulated by phosphorylation of nine sites on the Hec1 N-terminal tail. G) Fit decays from a cell expression phosophomutant 9A Hec1 (all phosphosites mutated to alanine) and 9D Hec1 (all phosphosites mutated to aspartic acid). H) Mean KMT lifetime from cells expressing phosphomutant Hec1 (error bars are standard error of the mean; WT n=22, 9A n=40, 1D (S55D) n=41, 2D (S44,55D) n=32, 3D (S15,44,55D) n=37, 9D n=41).

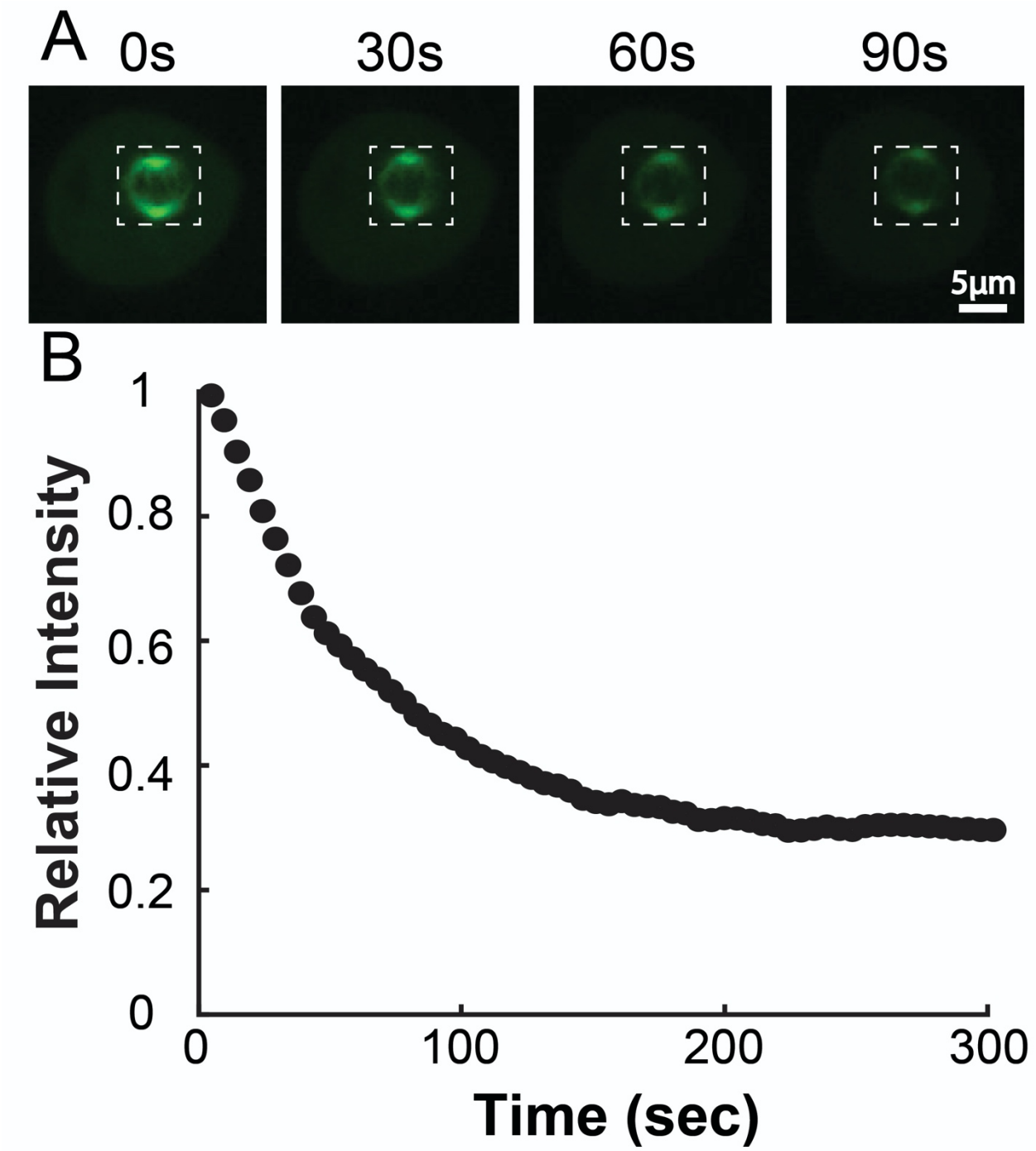

Figure 1 – supplement 1: mEOS3.2: α-tubulin bleaching correction curve. A) Time series of activated tubulin in spindles. The whole spindle was photoactivated with a 405nm laser and left to equilibrate for 5 minutes before imaging B) Mean integrated spindle intensity over time (boxed region). Curves were corrected for dark background by subtracting the mean intensity of a small region marked outside the cell. Curves from 13 cells were normalized to the initial intensity at t=0s and then averaged together.

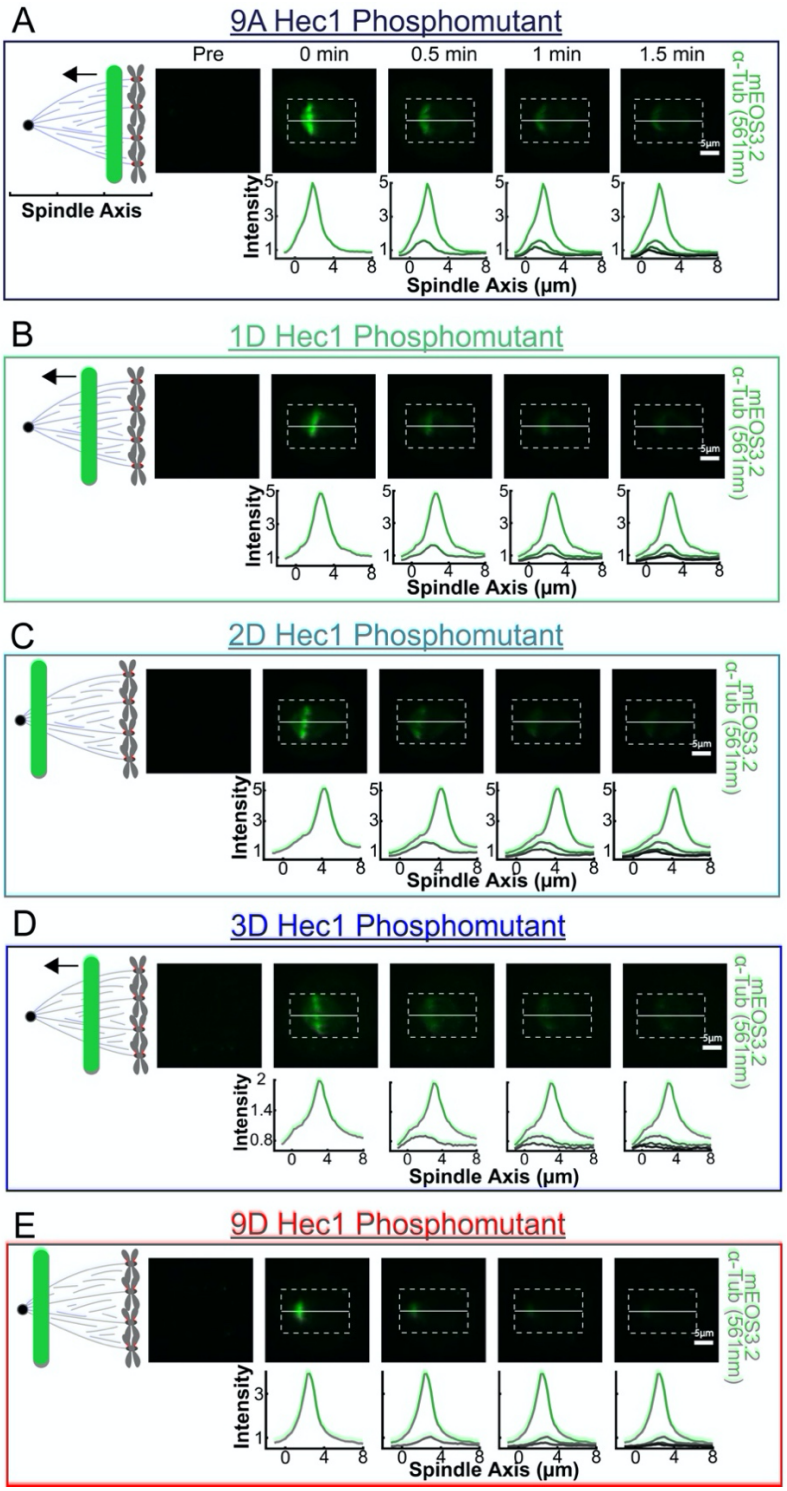

Figure 1 – supplement 2: Photoactivation line profiles for Hec1 Phosphomutants. A) Images from a photoconversion experiment in cells expressing a 9A-Hec1 Phosphomutant showing SNAP: mEOS3.2:α-tubulin (green). Images are shown immediately preceding, 0, 30, and 60s after photoconversion with a focused 405nm diode laser Line profile generated by averaging 3.5µm on either side of the spindle axis in the dotted box. B) 1D-Hec1 C) 2D-Hec1 D) 3D-Hec1 E) 9D-Hec1

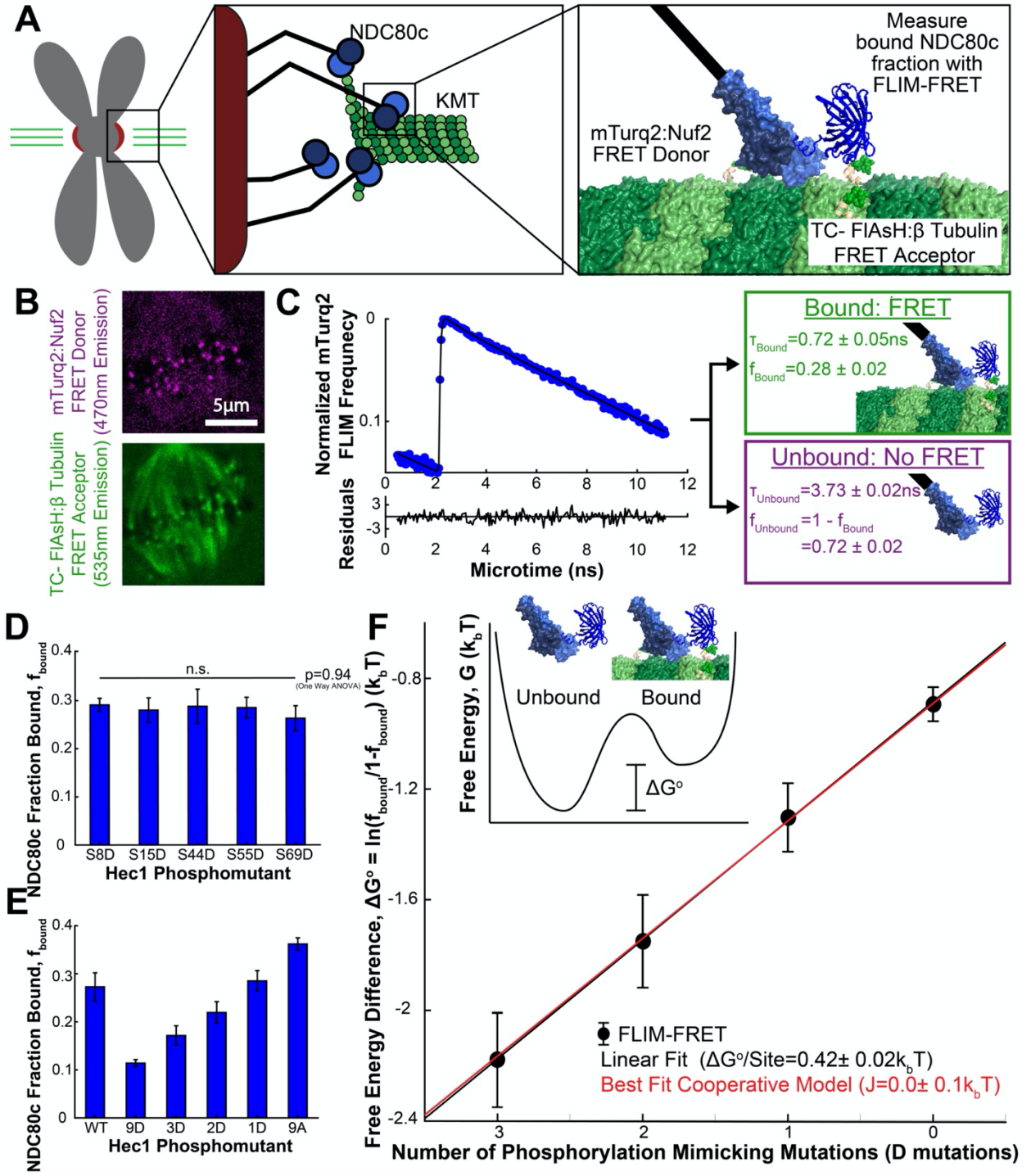

Figure 2: Measuring the fraction of NDC80c bound to KMTs with FLIM-FRET. A) NDC80c bound to KMTs with the Nuf2 subunit tagged with mTurquoise 2 and β-tubulin with a TC-FlAsH tag. B) mTurquoise2:Nuf2 FRET donor and the β-tubulin:TC-FlAsH FRET acceptor C) Normalized FLIM histogram of mTurquoise:Nuf2 localized at kinetochores fit a dual-exponential corresponding to the bound and unbound mTurquoise:Nuf2. D) Fraction of NDC80c bound to KMTs with phosphomutant S8D (n=12), S15D (n=12), S44D (n=12), S55D (n=18) and S69D (n=12) Hec1 (error bars are standard error of the mean). E) Fraction of NDC80c bound to

KMTs with phosphomutant WT (n=19), 9D (n=17), 3D (n=10), 2D (n=24), 1D (n=18) and 9A (n=24) Hec1. F) Free energy difference between bound and unbound NDC80c at kinetochores vs. the number of phosphorylation mimicking mutations. Black dots: FLIM-FRET experiment. Black line: linear fit. Red line: Cooperative model fit. The best fit cooperative contribution to the free energy, J, is indistinguishable from zero (p=0.99 Bayesian model comparison, see *Methods*). Inset: Free energy coordinate map of bound and unbound NDC80c

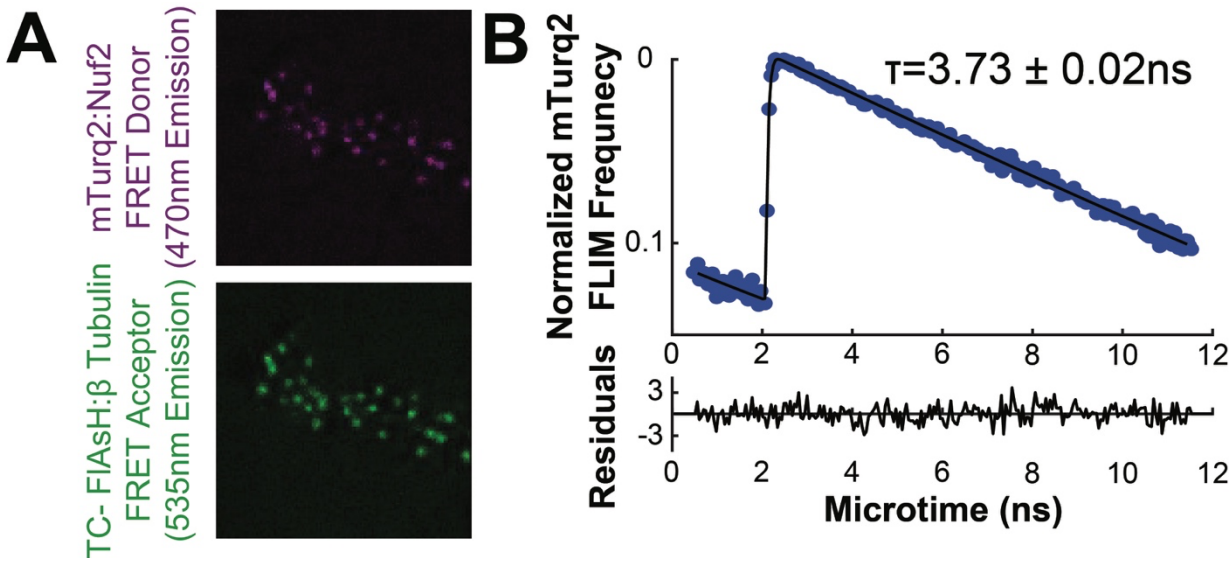

Figure 2 – supplement 1: FLIM curve of the mTurquoise2 FRET donor in the absence of the FlAsH FRET Acceptor. A) mTurqouise2:Nuf2 FRET donor and the β-tubulin:TC-FlAsH FRET acceptor channels B) Normalized FLIM histogram of mTurquoise:Nuf2 localized at kinetochores fit a single-exponential corresponding to only the non-FRET mTurquoise2.

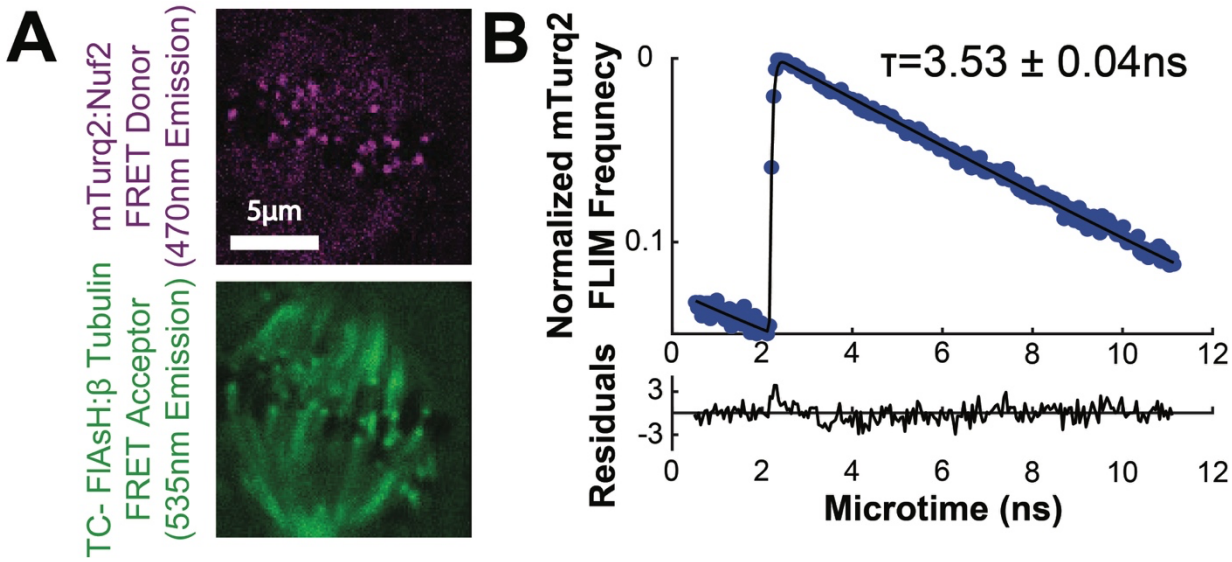

Figure 2 – supplement 2: FLIM curve of the mTurquoise2 FRET donor in the presence of the FlAsH FRET Acceptor fit to a single exponential decay. A) mTurqouise2:Nuf2 FRET donor and the β-tubulin:TC-FlAsH FRET acceptor channels B) Normalized FLIM histogram of mTurquoise:Nuf2 localized at kinetochores fit a single-exponential

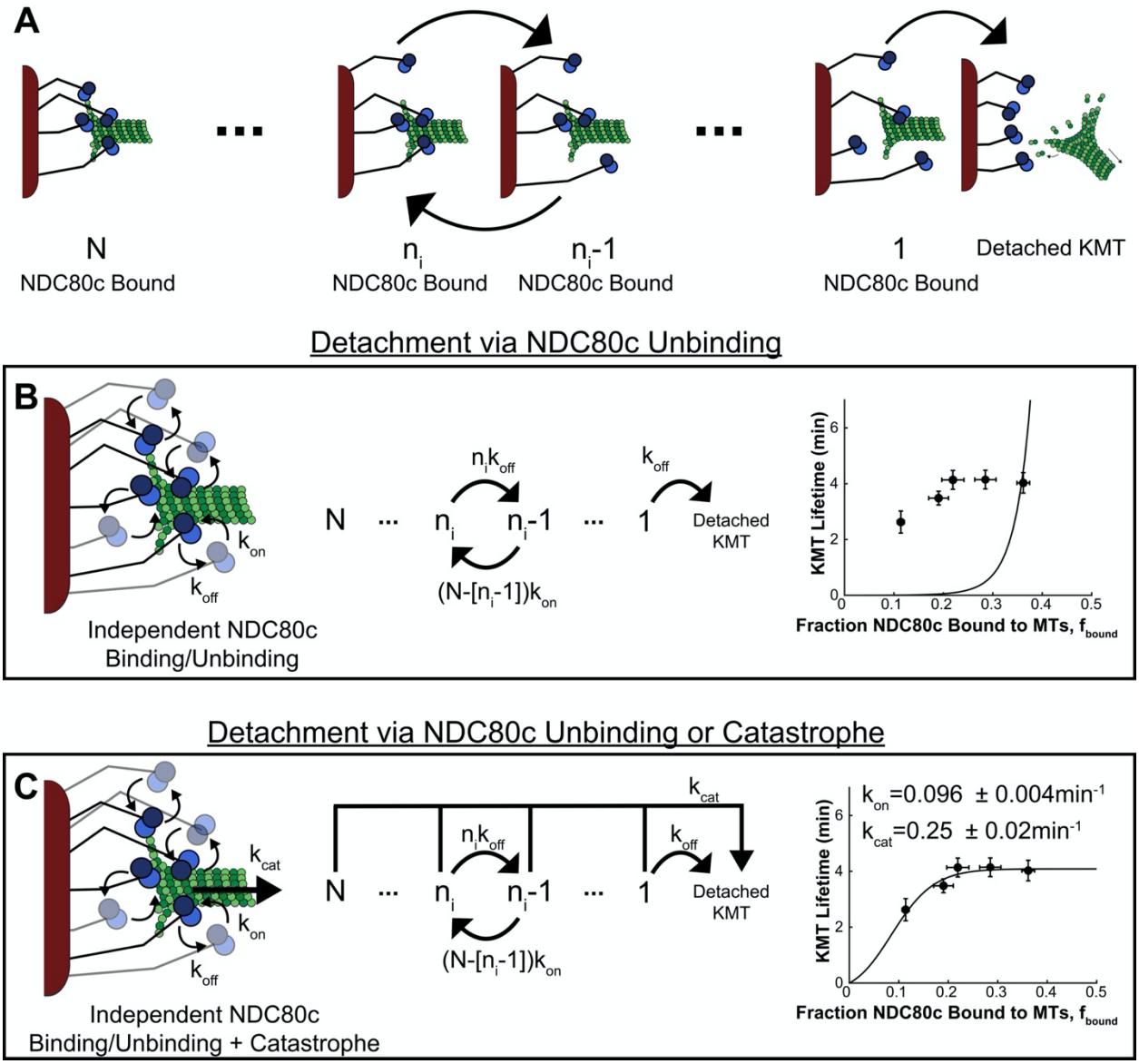

Figure 3: KMT detachment models. A) A rate transition model with states corresponding to the number of bound NDC80c with an additional state with the KMT detached. B) Left: A model with independent NDC80c binding and unbinding. Middle: Transitions between states defined only by NDC80c binding: $n_i \rightarrow n_{i-1}$: $n_i k_{off}$; $n_{i-1} \rightarrow n_i$: $n_{i-1} k_{on}$. The KMT detaches when the last NDC80c unbinds at rate k_{off}. Right: KMT Lifetime vs Fraction of NDC80c bound to MTs for Hec1 phosphomutants (black dots) compared with model predictions (black line). C) Left: A model with independent NDC80c binding and unbinding and KMT catastrophes. Middle: Transitions between states defined by NDC80c binding: $n_i \rightarrow n_{i-1}$: $n_i k_{off}$; $n_{i-1} \rightarrow n_i$: $n_{i-1} k_{on}$ and by KMT catastrophe: $n_i \rightarrow$ Detached: k_{cat} . Right: KMT Lifetime vs Fraction of NDC80c bound to MTs for Hec1 phosphomutants (black dots) compared with model predictions (black line)

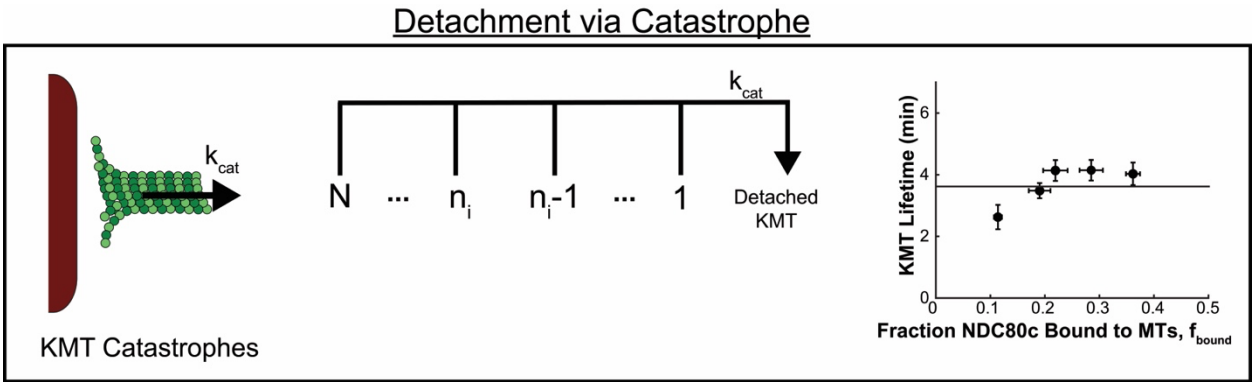

Figure 3 – supplement 1: KMT detachment from KMT catastrophes. Left: A model with only KMT catastrophes. Middle: Transitions between states defined by KMT catastrophe: $n_i \rightarrow$ Detached: k_{cat} . Right: KMT Lifetime vs Fraction of NDC80c bound to MTs for Hec1 phosphomutants (black dots) compared with model predictions (black line).

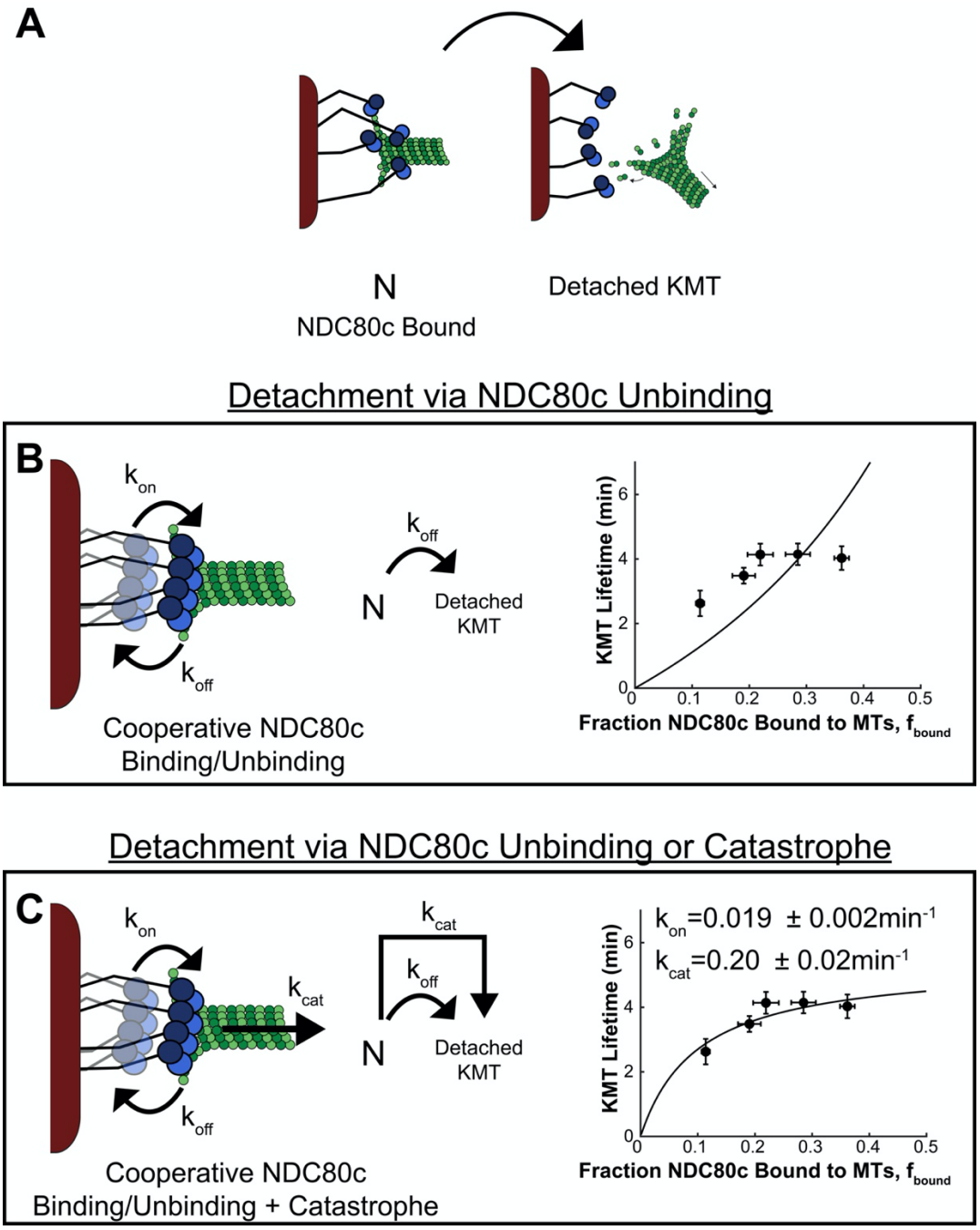

Figure 3 – supplement 2: KMT detachment models with cooperative NDC80c binding. A) A rate transition model with all NDC80c bound and a KMT detached state B) Left: A model with cooperative NDC80c binding and unbinding. Middle: Transitions between states defined only by NDC80c binding k_{off}. Right: KMT Lifetime vs Fraction of NDC80c bound to MTs for Hec1 phosphomutants (black dots) compared with model predictions (black line). C) Left: A model with cooperative NDC80c binding and unbinding and KMT catastrophes. Middle: Transitions between states defined by NDC80c binding: k_{off} and by KMT catastrophe: k_{cat} . Right: KMT Lifetime vs Fraction of NDC80c bound to MTs for Hec1 phosphomutants (black dots) compared with model predictions (black line)

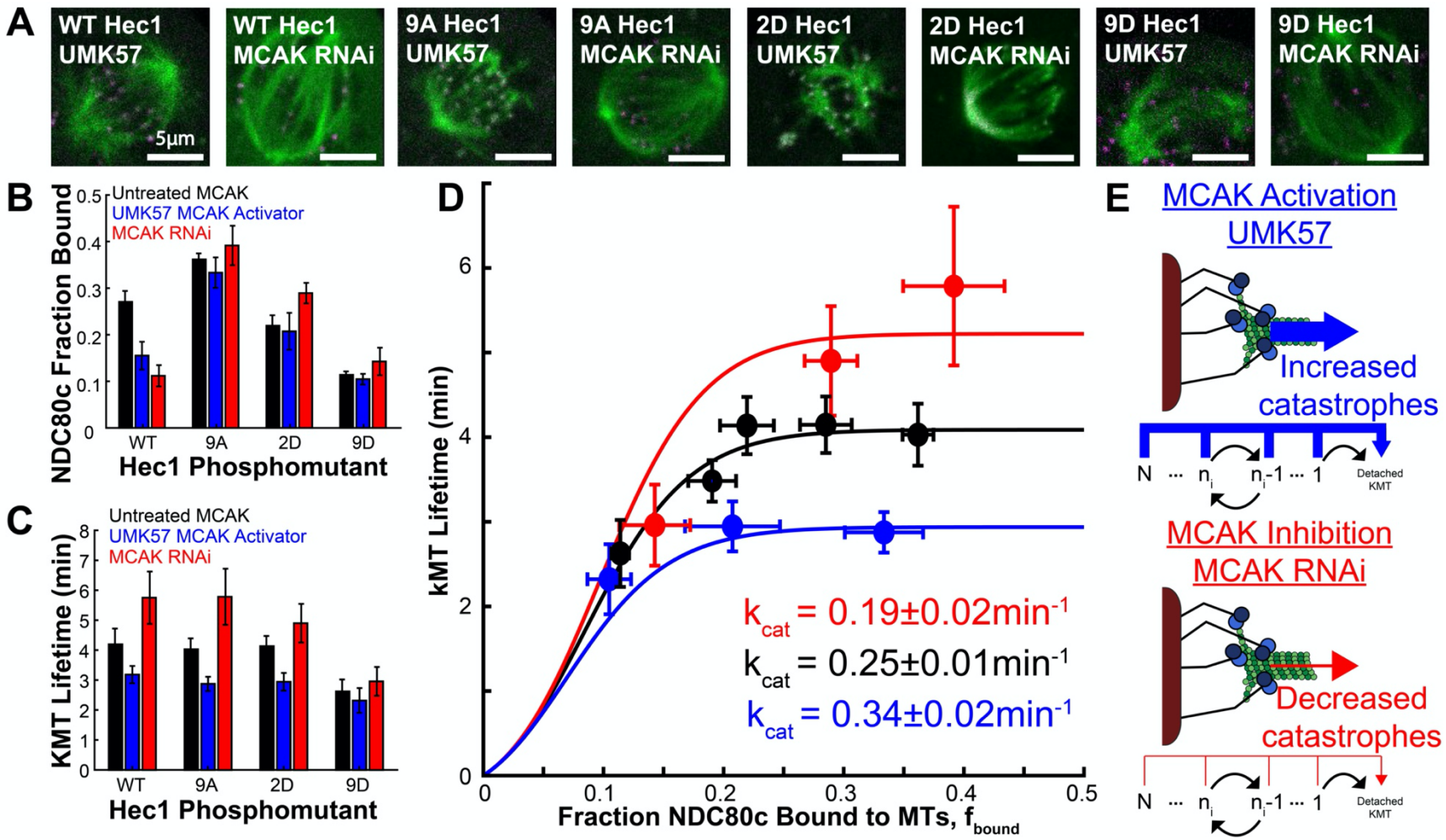

Figure 4: Both MCAK hyperactivation and depletion alter the KMT catastrophe rate. A) UMK57 treated and MCAK depleted cells with WT-,9A-,2D- and 9D-Hec1. B) NDC80c fraction bound for wild type MCAK (black), UMK57 treated hyperactivated MCAK (blue) and MCAK depleted (red) cells with WT-,9A-,2D- and 9D-Hec1 (error bars are standard error of the mean. Untreated: WT-Hec1 n=19, 9D-Hec1 n=17, 2D-Hec1 n=24, 9A-Hec1 n=24; MCAK RNAi: WT-Hec1 n=7, 9D-Hec1 n=7, 2D-Hec1 n=11, 9A-Hec1 n=11; UMK57 MCAK: WT-Hec1 n=12, 9D-Hec1 n=7, 2D-Hec1 n=12, 9A-Hec1 n=10). C) KMT lifetime for wild type MCAK (black), UMK57 treated hyperactivated MCAK (blue) and MCAK depleted (red) cells with WT-,9A-,2D- and 9D-Hec1. (Untreated:

WT-Hec1 n=22, 9D-Hec1 n=41, 2D-Hec1 n=32, 9A-Hec1 n=40; MCAK RNAi: WT-Hec1 n=16, 9D-Hec1 n=17, 2D-Hec1 n=21, 9A-Hec1 n=20; UMK57 MCAK: WT-Hec1 n=33, 9D-Hec1 n=19, 2D-Hec1 n=27, 9A-Hec1 n=31) D) KMT lifetime vs fraction of NDC80c bound to KMTs for cells expressing Hec1 phosphomutants with wild type (black dots) hyperactivated (blue dots) and depleted (red dots) MCAK fit to the dual detachment mechanism model (red, blue and black lines). E) MCAK hyperactivation with UMK57 increases the KMT catastrophe rate while MCAK inhibition with MCAK RNAi decreases the KMT catastrophe rate.

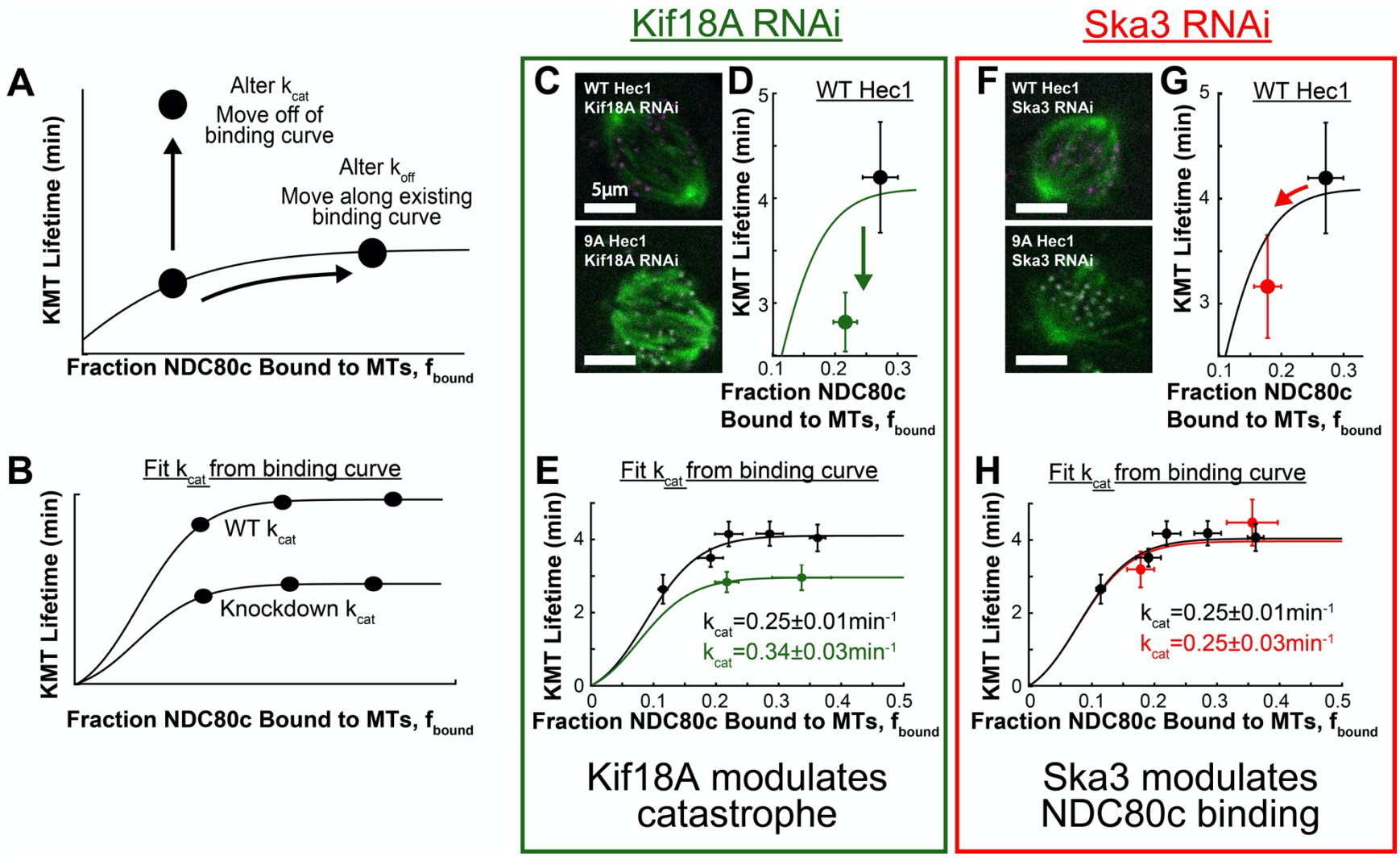

Figure 5: Role of Kif18a and Ska in regulating KMT stability. A) Schematic depicting the changes in KMT lifetime and NDC80c bound fraction from a change in k_{cat} (vertical motion off the fit detachment mechanism curve) or a change in k_{off} (motion along the existing dual detachment curve). B) Schematic depicting fitting the k_{cat} rate in the dual detachment mechanism to the KMT lifetime and fraction of NDC80c bound in Hec1 phosphomutants. C) Sample images for WT- and 9A-Hec1 phosphomutant cells treated with

Kif18A RNAi. D) Comparison of KMT lifetime and NDC80c bound fraction of WT-Hec1 cells treated with Kif18A RNAi (green) to untreated cells (black) E) Fit k_{cat}=0.34±0.03min^{-1} rate to WT- and 9A-Hec1 phosphomutants treated with Kif18A RNA (green) and untreated Hec1 phosphomutant cells (black) F) Sample images for WT- and 9A-Hec1 phosphomutant cells treated with Kif18A RNAi. G) Comparison of KMT lifetime and NDC80c bound fraction of WT-Hec1 cells treated with Kif18A RNAi (red) to untreated cells (black) H) Fit k_{cat}=0.25±0.03min^{-1} rate to WT- and 9A-Hec1 phosphomutants treated with Kif18A RNA (red) and untreated Hec1 phosphomutant cells (black);

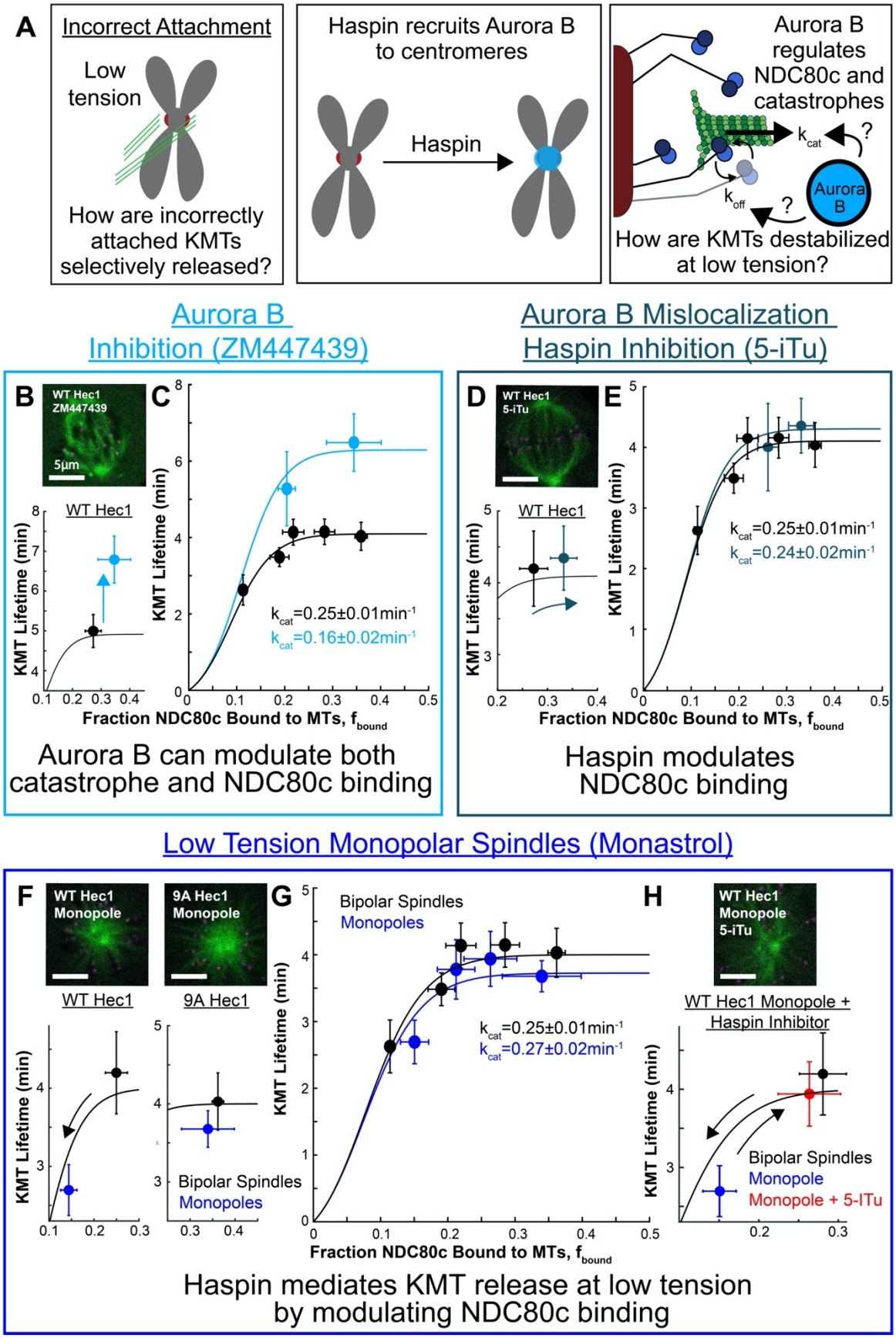
A
Incorrect Attachment
Low tension
How are incorrectly attached KMTs selectively released?
Haspin recruits Aurora B to centromeres
Haspin
Aurora B regulates NDC80c and catastrophes
k_{cat}
?
k_{off}
?
Aurora B
How are KMTs destabilized at low tension?
Aurora B Inhibition (ZM447439)
Aurora B Mislocalization Haspin Inhibition (5-iTu)
B
WT Hec1 ZM447439
5µm
WT Hec1
KMT Lifetime (min)
C
KMT Lifetime (min)
k_{cat}=0.25±0.01min^{-1}
k_{cat}=0.16±0.02min^{-1}
Fraction NDC80c Bound to MTs, f_{bound}
Aurora B can modulate both catastrophe and NDC80c binding
D
WT Hec1 5-iTu
WT Hec1
KMT Lifetime (min)
E
KMT Lifetime (min)
k_{cat}=0.25±0.01min^{-1}
k_{cat}=0.24±0.02min^{-1}
Fraction NDC80c Bound to MTs, f_{bound}
Haspin modulates NDC80c binding
Low Tension Monopolar Spindles (Monastrol)
F
WT Hec1 Monopole
9A Hec1 Monopole
WT Hec1
9A Hec1
KMT Lifetime (min)
Bipolar Spindles
Monopoles
G
Bipolar Spindles
Monopoles
KMT Lifetime (min)
k_{cat}=0.25±0.01min^{-1}
k_{cat}=0.27±0.02min^{-1}
Fraction NDC80c Bound to MTs, f_{bound}
H
WT Hec1 Monopole 5-iTu
WT Hec1 Monopole + Haspin Inhibitor
KMT Lifetime (min)
Bipolar Spindles
Monopole
Monopole + 5-ITu
Haspin mediates KMT release at low tension by modulating NDC80c binding

Figure 6: Low-tension KMTs are destabilized by a Haspin-mediated increase in the NDC80c unbinding k_{off} rate. A) Left: Schematic depicting a chromosome with low inter-kinetochore tension with both kinetochores attached to the same spindle pole. Middle: Haspin recruits the Aurora B kinase to the inner centromere by phosphorylating the H3T3 histone. Right: Aurora B can regulate either the NDC80c unbinding rate or the KMT catastrophe rate B) Sample image, KMT lifetime and NDC80c bound fraction of cells expressing WT-Hec1 and treated with ZM447439 Aurora B inhibitor (cyan) compared to untreated wild type (black) C) KMT lifetime and NDC80c bound fraction of WT- and 2D-Hec1 phosphomutants fit to the dual detachment mechanism for ZM447439 Aurora B inhibited cells (cyan, k_{cat}=0.16±0.02min^{-1}). D) Sample image, KMT lifetime and NDC80c bound fraction of cells expressing WT-Hec1 and treated with 5-ITu Haspin inhibitor compared to wild type E) KMT lifetime and NDC80c bound fraction of WT- and 2D-Hec1 phosphomutants fit to the dual detachment mechanism for 5-ITu Haspin inhibited cells (k_{cat}=0.14±0.02min^{-1}). F) Sample image, KMT lifetime and NDC80c bound fraction of monopolar spindles (treated with 200µM monastrol) expressing WT- and 9A-Hec1 compared to wild type bipolar spindles G) KMT lifetime and NDC80c bound fraction of monopolar phosphomutants fit to the dual detachment mechanism (k_{cat}=0.27±0.02min^{-1}). H) Sample image, KMT lifetime and NDC80c bound fraction of monopolar spindles expressing WT-Hec1 treated with 5-ITu Haspin inhibitor compared to wild type monopolar and bipolar spindles.

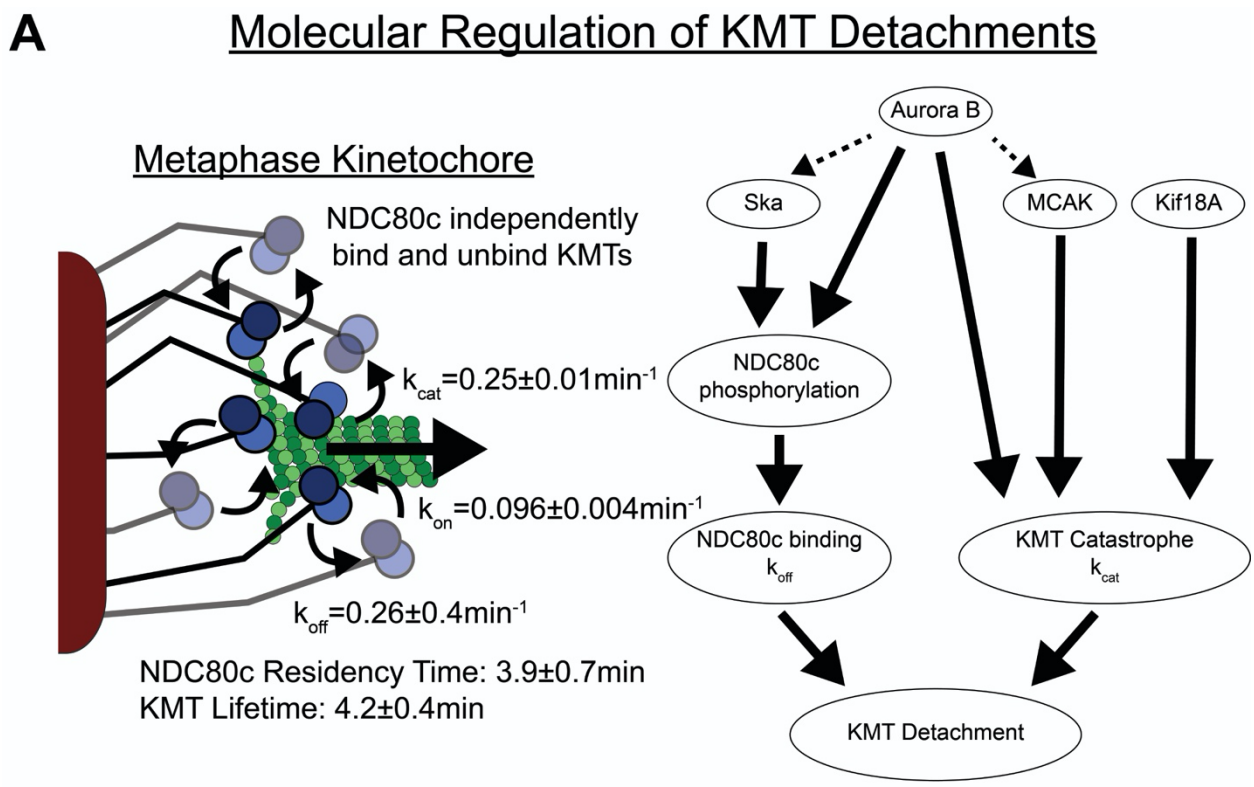
A
Molecular Regulation of KMT Detachments
Metaphase Kinetochore
NDC80c independently bind and unbind KMTs
k_{cat}=0.25±0.01min^{-1}
k_{on}=0.096±0.004min^{-1}
k_{off}=0.26±0.4min^{-1}
NDC80c Residency Time: 3.9±0.7min
KMT Lifetime: 4.2±0.4min
Aurora B
Ska
MCAK
Kif18A
NDC80c phosphorylation
NDC80c binding k_{off}
KMT Catastrophe k_{cat}
KMT Detachment

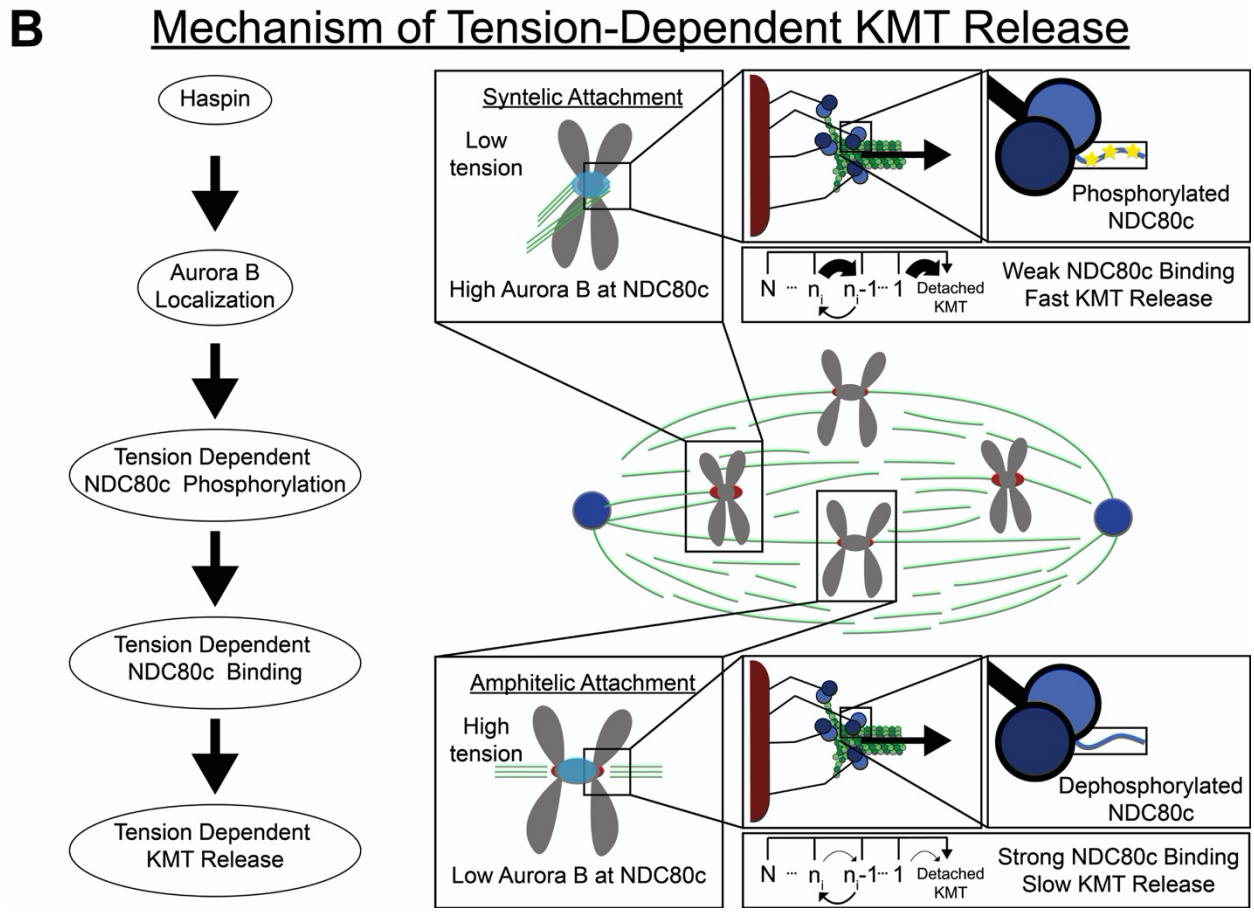
B
Mechanism of Tension-Dependent KMT Release
Haspin
Aurora B Localization
Tension Dependent NDC80c Phosphorylation
Tension Dependent NDC80c Binding
Tension Dependent KMT Release
Syntelic Attachment
Low tension
High Aurora B at NDC80c
Phosphorylated NDC80c
N ··· n_i n_i-1··· 1
Detached KMT
Weak NDC80c Binding
Fast KMT Release
Amphitelic Attachment
High tension
Low Aurora B at NDC80c
Dephosphorylated NDC80c
N ··· n_i n_i-1··· 1
Detached KMT
Strong NDC80c Binding
Slow KMT Release

Figure 7: Summary of KMT Detachment Regulation A) NDC80c at metaphase kinetochores bind independently to KMTs. KMTs detach from the kinetochore when either: 1. All the NDC80cs spontaneously unbind or 2) Following a KMT catastrophe. The NDC80c bind to MTs at rate k_{on}~0.1min^{-1} and unbind from KMTs at rate k_{off}~0.3min^{-1}. The KMT catastrophe rate k_{cat}~0.25min^{-1} The NDC80c remain bound to the KMT for an average of 3 minutes. KMTs remain attached to kinetochores for an average of ~4 minutes. Aurora B kinase regulates NDC80c phosphorylation, Ska activity, MCAK activity and the KMT catastrophe rate. Ska regulates NDC80c phosphorylation; MCAK and Kif18A regulate KMT catastrophes. The KMT detachment rate is determined by the NDC80c unbinding rate k_{off} and the KMT catastrophe rate k_{cat}. B) KMTs are destabilized at low tension by recruitment of Aurora B to centromeres by Haspin. Centromere-localized Aurora B phosphorylates NDC80c in a tension-dependent manner, which confers tension dependence to NDC80c binding and KMT release. Sister kinetochores with incorrect attachments that are not bioriented are under low tension with highly phosphorylated NDC80c, weak NDC80c binding to KMTs and fast KMT release. Sister kinetochores with correct amphitelic attachments are bioriented and under high tension with dephosphorylated NDC80c, strong NDC80c to KMTs and slow KMT release.

STAR METHODS

Resource Availability

Lead Contact

All reagent and material requests should be referred to William Conway: wconway@flatironinstitute.org.

Materials Availability

All plasmids generated in this study are available on AddGene: 82793. All cell lines are available upon request from the Needleman Lab.

Data Availability

All original code and data have been deposited at Dryad and is publicly available as of the date of publication. DOIs are listed in the key resources table. Any additional information required to reanalyze the data reported in this paper is available from the lead contact upon request.

Experimental Model and Subject Details

U2OS Cell Line

U2OS cells were acquired from ATCC and cultured in DMEM (ThermoFisher) supplemented with 10% tetracycline-free FBS (ThermoFisher) and Pen-Strep (ThermoFisher) in a humified incubator with 5% CO_2 maintained at 37°C. A stable cell line expressing mEOS3.2:alpha-tubulin and SNAP:centrin was generated and selected using blastcidin and hygromycin. A related series of cell lines expressing various phosphomutant Hec1:SNAP under the control of a doxycycline promoter in addition to mEOS3.2:alpha-tubulin and SNAP:centrin were generated and selected with puromycin, blastcidin and hygromycin. An additional U2OS cell line with overexpressed mTurqouise2:Nuf2 and endogenously tagged beta-tubulin::tetracyctline(TC) as described previously (Yoo et al. 2018) was utilized. A related series of cell lines expressing phosphomutant Hec1:LSS-mOrange under the control of a doxycycline promoter in addition to overexpressed mTurquoise2:Nuf2 and endogenously tagged beta-tubulin::TC were generated and selected using geneticin, blastcidin and hygromycin.

Method Details

Sample preparation and imaging conditions

Cells were plated onto coverglasses (GG-22-1.5-pdl, neuVitro) prior to experiments. Cells were preincubated in Fluorobrite DMEM (ThermoFisher) supplemented with 10mM HEPES for ~15min immediately prior to imaging, and then transferred to a custom-built coverslip heater

maintained at 37ºC during imaging. Cells were maintained in imaging media covered by mineral oil for ~1 hour during experiments.

Spinning Disk Confocal Imaging and Photoconversion

Photoconversion experiments were performed on a home built spinning disk confocal microscope (Nikon Ti2000, Yokugawa CSU-X1) with 488nm and 647nm lasers, an EMCCD camera (Hamamatsu) and a 60x oil immersion objective and controlled using a custom Labview program described previously (Conway et al. 2022). Two fluorescence channels were acquired every 5s with either 500ms exposure, 561nm excitation, 593/40nm emission or 300ms exposure, 647nm excitation, 647 long pass emission in a single z plane for both channels. The mEOS3.2 was photoconverted using a 405nm diode laser aligned to a diffraction limited spot in the imagining plane of the microscope. The spot was moved across the sample at 5µm/s at a power of 500nW (measured at the objective) using a PI-Xynano piezo P-545 PiNano XYZ; Physik Instrumente) to draw a photoconverted line across the spindle. Prior to experiments, cells were stained with 500nM SNAP-Sir (New England Biolabs) for 30 minutes and then recovered in culture media for at least 4 hours.

All quantitative analysis was performed using a custom MATLAB GUI described previously (Conway et al. 2022). We defined the spindle axis by tracking both poles and fitting a line between them. We then generated a line profile by summing over 3.5µm on either side of the spindle axis and fit the profile to a gaussian. The height of the peak was determined by subtracting the height of the fit gaussian from the height of a gaussian fit to the opposite side of the spindle to correct for background. The peak heights were then corrected for bleaching by dividing by a bleaching calibration curve. To measure the bleaching calibration curve, the entire spindle was photoconverted and then left to equilibrate for 5 minutes. The spindles were then imaged using the same imaging conditions as the photoconversion experiments. The mean intensity inside an ROI around the spindle was determined and averaged over 13 cells and subtracted the mean of a region outside of the cell to correct for the dark noise of the camera. We then divided the peak intensity vs time curve by the bleaching calibration curve to produce a bleaching-corrected intensity curve.

Fluorescence Lifetime Imaging Microscopy – Fluorescence Resonance Energy Transfer (FLIM-FRET) Experiments

Fluorescence lifetime imaging microscopy (FLIM) experiments were performed on a home built two photon microscope as described previously (Yoo et al. 2018). Prior to experiments cells were stained with 1µM FlAsH-EDT_2 (ThermoFisher) in OPTIMEM for 2 hours, destained with 250µM EDT (Alfa Aesar) for 10 minutes, washed twice with OPTIMEM and then placed in culture media to recover for 6-10 hours. During imaging, cells were placed in a custom-built heating chamber and maintained at 37ºC in imaging media for roughly one hour. Cells were continuously excited using an 80MHz Ti:Sapphire pulsed laser (Insight X3, MKS) tuned to 865nm using a galvanometer scanner (DCS-120, Becker-Hickl) with a 40x water immersion objective (CFI Apo 40x WI, NA 1.25, Nikon) for a total of 3 minutes of acquisition time split into 3s frames. FLIM signal was recorded using a TCPSC module (SPC-150, Beck-Hickl) with two hybrid detectors (HPM-100, Becker-Hickl). A dichroic beam splitter (FF506-Di03) split the emission signal between the two detectors. A 470/24nm bandpass emission filter was mounted on one detector and

a 535/30nm bandpass filter on the other to record emission from mTurquoise2 and FlAsH respectively.

Quantitative FLIM analysis was performed using a custom MATLAB GUI described previously (Yoo et al. 2018). Kinetochores were tracked in the mTurqouise2 channel using the Kilfoil tracking algorithm (Gao and Kilfoil 2009). The photons from each kinetochore pixel were then binned to a single FLIM decay curve for analysis and fit to a dual exponential using a Bayesian algorithm described previously (Kaye at al. 2017, Yoo et al. 2018). The long lifetime of the dual exponential was fixed to 3.73ns, determined by fitting an mTurquoise2 FLIM decay curve from unstained cells to a single exponential. The fraction of NDC80c bound to KMTs was calculated by dividing the slow decay fraction from the fit dual exponential by a correction factor or 0.42 to account for the fraction of tubulin that was stained with the FlAsH FRET acceptor.

Calculating the equilibrium constant K for a cooperative two state system

We calculated the fraction of NDC80c bound to KMTs in a cooperative two-state system using the system's partition function (Kardar et al. 2007). We included 21 model states ranging from no NDC80c bound to all N=20 NDC80c bound to the KMT. We defined a Hamiltonian, H, for the state with i NDC80c bound that included both a binding energy between NDC80c and KMTs, ε, and a pairwise, cooperative interaction energy between the NDC80cs bound KMTs, J: $H = -i\varepsilon - \binom{i}{2}J = -i\varepsilon - \frac{i(i-1)}{2}J$. The partition function, Z, then becomes:

$$Z = \sum_{i=0}^{N} \rho(i) e^{-\beta H} = \sum_{i=0}^{N} \binom{N}{i} e^{-\beta i\varepsilon - \beta\frac{i(i-1)}{2}J}$$

And the equilibrium constant K is:

$$K = \frac{n_{Bound}}{N - n_{Bound}} = \frac{\frac{1}{Z}\sum_{i=0}^{N} i \binom{N}{i} e^{-\beta i\varepsilon - \beta\frac{i(i-1)}{2}J}}{N - \frac{1}{Z}\sum_{i=0}^{N} i \binom{N}{i} e^{-\beta i\varepsilon - \beta\frac{i(i-1)}{2}J}}$$

In the case where there is no binding cooperativity (J=0), the equilibrium constant reduces to the familiar expression for an uncooperative two-state model:

$$K = \frac{\frac{1}{Z}\sum_{i=0}^{N} i \binom{N}{i} e^{-\beta i\varepsilon}}{N - \frac{1}{Z}\sum_{i=0}^{N} i \binom{N}{i} e^{-\beta i\varepsilon}} = e^{-\beta\varepsilon}$$

We defined an effective free energy difference between the states ΔG (Silbey et al. 2005):

$$\Delta G = k_B T \ln K$$

To fit the expression for the free energy difference to experimental data, we assumed that each additional phosphomutation changed the NDC80c-KMT binding energy ε by the same amount, $\Delta\varepsilon$/site, and that the NDC80c-NDC80c interaction energy J was the same for each phosphomutant

(Zaystev et al 2015), which resulted in three fitting parameters: J, $\Delta\varepsilon$/site, and ε_{9A}, the binding energy of the 9A-Hec1 phosphomutant. We then calculated the predicted ΔG for each of the phosphomutants for a given J, $\Delta\varepsilon$/site, and ε_{9A} and fit these values to the free energy differences we measured in the FLIM-FRET experiment by minimizing a χ^2 statistic. We found the best fit at J=0.0 ± 0.1k_BT, which was not significantly improved from a fit to the uncooperative model, where J is fixed to 0 (p=0.99 Bayesian model comparison).

Expression of Hec1 phosphomutants with siRNA knockdown and doxycycline-induced mutant expression

U2OS cells were plated at 50% confluency in T75 flasks (ThermoFisher) in DMEM supplemented with 10% tetracycline-free FBS and PenStrep. We used a Flexitube siRNA duplex targeted to the 5' UTR of the Hec1 gene (5'-TCCCTGGGTCGTGTCAGGAAA-3', QIAGEN Hs_KNTC2_7 SI02653567) to knockdown endogenous Hec1. 240pmol of siRNA and 8µL of Lipofectamine RNAiMax (ThermoFisher 13778030) were separately incubated in two tubes of 1.2mL of OPTIMEM (ThermoFisher) for 5 minutes at room temperature and then combined and incubated for an additional 30 minutes of incubation. The DMEM media was replaced with 8mL of OPTIMEM supplemented with 10% tetracycline-free FBS. The siRNA-Lipofectamine cocktail was then added dropwise to the cell culture media. Cells were incubated with the siRNA media for 24 hours. We then washed the siRNA off and split the cells to six 35mm dishes containing 25mm poly-D-lysine coated coverslips and 2mL of DMEM supplemented with 10% tetracycline-free FBS supplemented with PenStrep and 2µg/mL of doxycycline to induce phosphomutant Hec1 expression for 24 hours before imaging. For experiments where additional genes were knocked down, a dual cocktail containing 240pmol of each siRNA and 16µL of Lipofectamine RNAiMAX incubated in 1.2mL of OPTIMEM was used.

Mathematical Modeling of KMT Detachment

We developed a Markov chain transition model to describe a KMT interacting with N=20 NDC80c. We included 21 model states ranging from no NDC80c bound to all 20 NDC80c bound to the KMT. In a model where transitions between the states are determined solely by NDC80c binding, the transition matrix between the states T is:

$$\begin{bmatrix} 1-\mathrm{Nk_{off}} & \mathrm{Nk_{off}} & 0 & \cdots & 0 & 0 \\ \mathrm{k_{on}} & 1-(\mathrm{N}-1)\mathrm{k_{off}}-\mathrm{k_{on}} & (\mathrm{N}-1)\mathrm{k_{off}} & \cdots & 0 & 0 \\ 0 & 2\mathrm{k_{on}} & \ddots & \ddots & \ddots & \vdots \\ \vdots & \vdots & \ddots & \ddots & 2\mathrm{k_{off}} & 0 \\ 0 & 0 & \ddots & (\mathrm{N}-1)\mathrm{k_{on}} & 1-\mathrm{k_{off}}-(\mathrm{N}-1)\mathrm{k_{on}} & \mathrm{k_{off}} \\ 0 & 0 & \cdots & 0 & 0 & 1 \end{bmatrix}$$

Which can be expressed in block form as:

$$\begin{bmatrix} & & & 0 \\ & \mathbf{Q} & & \vdots \\ & & & \mathrm{k_{off}} \\ 0 & \cdots & 0 & 1 \end{bmatrix}$$

The mean first passage time from each of the 20 n_i NDC80c bound states to the absorbing 0 NDC80c bound state is given by $(1-Q)^{-1}\vec{\mathbf{1}}$, where $\vec{\mathbf{1}}$ is a column vector composed entirely of ones. (Allen et al. 2010). Treating the non-absorbing states in steady state, the probability distribution of the number of NDC80c initially bound is given by a binomial distribution, $p_{eq}(n_i) = \binom{N}{n_i}(\frac{k_{off}}{k_{off}+k_{on}})^{n_i}(\frac{k_{on}}{k_{off}+k_{on}})^{N-n_i}$. Multiplying the probability of beginning in each state p_{eq} by the mean first passage time from each state to the absorbing state and summing gives the mean time for the KMT to detach:

$$\tau = p_{eq}(1-Q)^{-1}\vec{\mathbf{1}}$$

Incorporating unbind by KMT catastrophe is accomplished by adding a transition from each state to the 0 NDC80c bound detached state at rate k_{cat}. The transition matrix is then:

$$\begin{bmatrix} 1-\mathrm{Nk_{off}}-\mathrm{k_{cat}} & \mathrm{Nk_{off}} & 0 & \cdots & 0 & \mathrm{k_{cat}} \\ \mathrm{k_{on}} & 1-(\mathrm{N}-1)\mathrm{k_{off}}-\mathrm{k_{on}}-\mathrm{k_{cat}} & (\mathrm{N}-1)\mathrm{k_{off}} & \cdots & 0 & \mathrm{k_{cat}} \\ 0 & 2\mathrm{k_{on}} & \ddots & \ddots & \ddots & \vdots \\ \vdots & \vdots & \ddots & \ddots & 2\mathrm{k_{off}} & \mathrm{k_{cat}} \\ 0 & 0 & \ddots & (\mathrm{N}-1)\mathrm{k_{on}} & 1-\mathrm{k_{off}}-(\mathrm{N}-1)\mathrm{k_{on}}-\mathrm{k_{cat}} & \mathrm{k_{off}}+\mathrm{k_{cat}} \\ 0 & 0 & \cdots & 0 & 0 & 1 \end{bmatrix}$$

Quantification and Statistical Analysis

The number of cells analyzed in each condition can be found in the figure legends. Error bars are always standard error of the mean.

Key Resource Table

REAGENT or RESOURCE	SOURCE	IDENTIFIER
Chemicals, peptides, and recombinant proteins		
DMEM	ThermoFisher	Cat # 10566016
Tet-system approved FBS	ThermoFisher	Cat # A4736401
Pen-Strep	ThermoFisher	Cat # 15070063
PBS	ThermoFisher	Cat # 70011044
Trypsin	ThermoFisher	Cat # 25200056
Lipofectamine RNAiMax	ThermoFisher	Cat#:13778075
Doxycycline	ThermoFisher	Cat #: AAJ60579-14
FlAsH-EDT2	ThermoFisher	Cat#:T34561
1,2-Ethanedithiol (EDT)	Alfa Aesar	Cat#:540-63-6
SNAP-Cell® 647-SiR	NEB	Cat # S9102S
Fluorobrite DMEM	ThermoFisher	Cat # A1896701
HEPES, 1M	ThermoFisher	Cat # 15630080
ZM447439	Enzo Life Sciences	Cat#:BML-EI373
5-iodotubercidin (5-ITu)	Enzo Life Sciences	Cat#:BML-EI29
Monastoral	SeleckChem	Cat #: S8439

Deposited data		
Photoactivation and FLIM-FRET Experiments	Dryad	
Experimental models: Cell lines		
U2OS cells expressing mEOS3.2:alpha-tubulin and SNAP:centrin	This paper	
U2OS cells expressing mEOS3.2:alpha-tubulin and SNAP:centrin + doxycycline inducible 9A-Hec1:SNAP	This paper	
U2OS cells expressing mEOS3.2:alpha-tubulin and SNAP:centrin + doxycycline inducible 1D-Hec1:SNAP	This paper	
U2OS cells expressing mEOS3.2:alpha-tubulin and SNAP:centrin + doxycycline inducible 2D-Hec1:SNAP	This paper	
U2OS cells expressing mEOS3.2:alpha-tubulin and SNAP:centrin + doxycycline inducible 3D-Hec1:SNAP	This paper	
U2OS cells expressing mEOS3.2:alpha-tubulin and SNAP:centrin + doxycycline inducible 9D-Hec1:SNAP	This paper	
U2OS cells expressing beta-Tubulin:TC and mTurquoise2:Nuf2	Yoo et al. 2018	
U2OS cells expressing beta-Tubulin:TC and mTurquoise2:Nuf2 + doxycycline inducible 9A-Hec1: LSSmOrange	This paper	
U2OS cells expressing beta-Tubulin:TC and mTurquoise2:Nuf2 + doxycycline inducible 1D-Hec1: LSSmOrange	This paper	
U2OS cells expressing beta-Tubulin:TC and mTurquoise2:Nuf2 + doxycycline inducible 2D-Hec1: LSSmOrange	This paper	
U2OS cells expressing beta-Tubulin:TC and mTurquoise2:Nuf2 + doxycycline inducible 3D-Hec1: LSSmOrange	This paper	
U2OS cells expressing beta-Tubulin:TC and mTurquoise2:Nuf2 + doxycycline inducible 9D-Hec1: LSSmOrange	This paper	
Oligonucleotides		
NDC80c RNAi	Qiagen	5'-TCCCTGGGTCGTGTCAGGAAA
MCAK RNAi	Dharmacon	50-50 Mix of: 5'-GCAGGCUAGCAGACAAAUUU and 5'-GAUCCAACGCAGUAAUGGUUU
Kif18A RNAi	Dharmacon	5'-GCCAAUUCUUCGUAGUUUU
Ska3 RNAi	Qiagen	5'-AACAGAATGGTTTAAGTAGTA
Software and algorithms		
Matlab 2020b	Mathworks	-
FLIM-FRET Data Analysis GUI	Yoo et al. 2018	-
Photoactivation Data Analysis GUI	Conway et al. 2022	-
Other		
Poly-d-lysine coated coverslips for imaging	NeuVitro	GG-25-15-PDL

Custom cell heater for imaging	Bioscience Tools	-

REFERENCES

Abad MA, Medina B, Santamaria A, Zou J, Plasberg-Hill C, Madhumalar A, Jayachandran U, Redli PM, Rappsilber J, Nigg EA, et al. (2014) "Structural basis for microtubule recognition by the human kinetochore Ska complex." Nat Commun. 5:2964. 10.1038/ncomms3964

Algar, W., Hildebrandt, N., Vogel, S., Medintz, I. (2019). "FRET as a biomolecular research tool — understanding its potential while avoiding pitfalls" Nat Meth. 16: pp. 815-829. DOI: 10.1038/s41592-019-0530-8

Allen, L. An introduction to stochastic processes with applications to biology. CRC Press, 2010.

Andresen M, Schmitz-Salue R, Jakobs S. (2004) "Short tetracysteine tags to beta-tubulin demonstrate the significance of small labels for live cell imaging." Molecular Biology of the Cell 15:5616–5622. DOI: 0.1091/mbc.e04-06-0454.

Andrews, P.D., Y. Ovechkina, N. Morrice, M. Wagenbach, K. Duncan, L. Wordeman, and J.R. Swedlow. (2004) "Aurora B regulates MCAK at the mitotic centromere." Dev. Cell. 6:253–268. DOI: 10.1016/S1534-5807(04)00025-5

Akiyoshi B., Sarangapani K.K., Powers A.F., Nelson C.R., Reichow S.L., Arellano-Santoyo H., Gonen T., Ranish J.A., Asbury C.L., Biggins S. (2010). "Tension Directly Stabilizes Reconstituted Kinetochore-Microtubule Attachments." Nature. 468:576–579. DOI: 10.1038/nature09594.

Auckland P., Clarke N.I., Royle S.J., McAinsh A.D. (2017) "Congressing Kinetochores Progressively Load Ska Complexes to Prevent Force-Dependent Detachment." J. Cell Biol. 216:1623–1639. DOI: 10.1083/jcb.201607096..

Bakhoum, S. F., Thompson, S. L., Manning, A. L., and Compton, D. A. (2009). Genome Stability Is Ensured by Temporal Control of Kinetochore-Microtubule Dynamics. Nat. Cel Biol. 11, 27–35. Doi:10.1038/ncb1809

Barbosa J, Sunkel CE, Conde C. (2022). "The Role of Mitotic Kinases and the RZZ Complex in Kinetochore-Microtubule Attachments: Doing the Right Link." Front Cell Dev Biol. 10:787294. Doi: 10.3389/fcell.2022.787294.

Broad A.J., DeLuca J.G. (2020). "The right place at the right time: Aurora B kinase localization to centromeres and kinetochores." Essays Biochem. 64:299–311. Doi: 10.1042/EBC20190081.

Carmena M, Wheelock M, Funabiki H, Earnshaw WC. (2012). "The chromosomal passenger complex (CPC): from easy rider to the godfather of mitosis." Nat Rev Mol Cell Biol. 13(12):789-803. Doi: 10.1038/nrm3474.

Cheeseman IM, Chappie JS, Wilson-Kubalek EM, Desai A. The conserved KMN network constitutes the core microtubule-binding site of the kinetochore. Cell. 2006;127:983–997.

Cheeseman, I., Desai, A. (2008). “Molecular architecture of the kinetochore–microtubule interface.” Nat Rev Mol Cell Biol 9, 33–46 DOI: 10.1038/nrm2310

Daum JR, Wren JD, Daniel JJ, Sivakumar S, McAvoy JN, Potapova TA, Gorbsky GJ.(2009). “Ska3 is required for spindle checkpoint silencing and the maintenance of chromosome cohesion in mitosis.” Curr Biol. 19:1467–72. DOI:

Chen GY, Renda F, Zhang H, Gokden A, Wu DZ, Chenoweth DM, Khodjakov A, Lampson MA. (2021). “Tension promotes kinetochore-microtubule release by Aurora B kinase.” J Cell Biol.;220(6):e202007030. Doi: 10.1083/jcb.202007030.

de Regt AK, Clark CJ, Asbury CL, Biggins S (2022). “Tension can directly suppress Aurora B kinase-triggered release of kinetochore-microtubule attachments.” Nat Commun. 13(1):2152. Doi: 10.1038/s41467-022-29542-8.

DeLuca J, et al. Kinetochore microtubule dynamics and attachment stability are regulated by Hec1. Cell. 2006;127:969–982.

DeLuca, J. (2010). “Chapter 4 – Kinetochore–Microtubule Dynamics and Attachment Stability”, Meth Cell Biol, 97, pp.53-69. Doi: 10.1016/S0091-679X(10)97004-0.

DeLuca K, Lens SM, DeLuca JG (2011). Temporal changes in Hec1 phosphorylation control kinetochore-microtubule attachment stability during mitosis. J Cell Sci. pp. 124:622–634. DOI: 10.1242/jcs.072629.

Ditchfield C, Johnson VL, Tighe A, Ellston R, Haworth C, Johnson T, Mortlock A, Keen N, Taylor SS. (2003). “Aurora B couples chromosome alignment with anaphase by targeting BubR1, Mad2, and Cenp-E to kinetochores.” J Cell Biol. Apr 28;161(2):267-80. Doi: 10.1083/jcb.200208091.

DeLuca, K., Meppelink, A., Broad, A., Mick, J., Peersen, O., Pektas, S., Lens, S., DeLuca, J. (2018). “Aurora A kinase phosphorylates Hec1 to regulate metaphase kinetochore–microtubule dynamics.” 217 (1): 163–177. DOI: 10.1083/jcb.201707160

Domnitz, S., Wagenbach, M., Decarreau, J., Wordeman, L. (2012) “MCAK activity at microtubule tips regulates spindle microtubule length to promote robust kinetochore attachment.” J Cell Biol. 197(2): 231-7. DOI: 10.1083/jcb.201108147

Edson, K., Payton, M. (2022) “Targetting the mitotic kinesin Kif18A in chromosomally unstable cancers: hit optimization towards an in vivo chemical probe”. J Med Chem. 65(6): 4972-4990. DOI: 10.1021/acs.jmedchem.1c02030

Edzuka, T., Goshima, G. (2018). “Drosophila kinesin-8 stabilizes the kinetochore–microtubule interaction.” J. Cell Biol. 218, 474–488. DOI: 10.1083/jcb.201807077

Ems-McClung, S., Hainline, S., Devare, J., Zong, H., Cai, S., Carnes, S., Shaw, S., Walczak, C.E. (2013). “Aurora B Inhibits MCAK Activity through a Phosphoconformational Switch that Reduces Microtubule Association.” *Curr Biol.* 23 (24 2492). DOI: 10.1016/j.cub.2013.10.054.

Gaitanos TN, Santamaria A, Jeyaprakash AA, Wang B, Conti E, Nigg EA. (2009) “Stable kinetochore-microtubule interactions depend on the Ska complex and its new component Ska3/C13Orf3.” Embo J. 28:1442–52. DOI:

Gao, Y., Kilfoil, M. (2009). “Accurate detection and complete tracking of large populations of features in three dimensions”, Optics Express, 17(6), pp. 4685-4704. Doi: 10.1364/OE.17.004685

Godek, K., Kabeche, L., Compton D. (2015) “Regulation of kinetochore-microtubule attachments through homeostatic control during mitosis” Nature Reviews Molecular Cell Biology 16, pp. 57–64. Doi: 10.1038/nrm3916.

Hanisch A., Silljé H.H.W., Nigg E.A. (2006) :Timely Anaphase Onset Requires a Novel Spindle and Kinetochore Complex Comprising Ska1 and Ska2.” EMBO J. 25:5504–5515. DOI: 10.1038/sj.emboj.7601426.

Hara, Masatoshi & Fukagawa, Tatsuo. (2020). “Dynamics of kinetochore structure and its regulations during mitotic progression.” Cellular and Molecular Life Sciences. 77. DOI: 10.1007/s00018-020-03472-4.

Hayward, D., Roberts, E., Gruneberg, U. (2022). “MPS1 localizes to end-on microtubule-attached kinetochores to promote microtubule release.” Curr Biol. 32 pp. 5200-5208. DOI: 10.1016/j.cub.2022.10.047.

Hunter A. W., Caplow M., Coy D. L., Hancock W. O., Diez S., Wordeman L., and Howard J. (2003). “The kinesin-related protein MCAK is a microtubule depolymerase that forms an ATP-hydrolyzing complex at microtubule ends.” Mol. Cell 11, 445-457. DOI: 10.1016/S1097-2765(03)00049-2.

Hoffmann C, Gaietta G, Bunemann M, Adams SR, Oberdorff-Maass S, Behr B, Vilardaga JP, Tsien RY, Ellisman MH, Lohse MJ. (2005) “A FlAsH-based FRET approach to determine G protein-coupled receptor activation in living cells”. Nature Methods 2:171–176. DOI: 10.1038/nmeth742.

Janczyk P, Skorupa KA, Tooley JG, Matson DR, Kestner CA, West T, Pornillos O, Stukenberg PT, (2017). “Mechanism of Ska Recruitment by Ndc80 Complexes to Kinetochores.” Developmental Cell. 41(4) 438-449. DOI:

Joglekar A. P. and Kukreja A. A. (2017). “How kinetochore architecture shapes the mechanisms of its function.” Curr. Biol. 27, R816-R824. DOI: 10.1016/j.cub.2017.06.012

Kabeche, L., Compton, D. (2013). “Cyclin A Regulates Kinetochore-Microtubules to Promote Faithful Chromosome Segregation”, 502(7469): 110–113.doi: 10.1038/nature12507.

Kapoor, T.M., T.U. Mayer, M.L. Coughlin, and T.J. Mitchison. (2000). “Probing spindle assembly mechanisms with monastrol, a small molecule inhibitor of the mitotic kinesin”, Eg5. J. Cell Biol. 150:975–988.

Kardar, M. (2007). “Statistical Physics of Particles”. Camrbrdige University Press.

Kaye B., Foster PJ, Yoo TY, Needleman DJ. (2017) “Developing and testing a Bayesian analysis of fluorescence lifetime measurements” Plos One 12:e0169337. DOI: 10.1371/journal.pone.0169337

Kaye, B., Stiehl, O., Foster, PJ, Shelley, M., Needleman, D. (2018). “Measuring and modeling polymer concentration profiles near spindle boundaries argues that spindle microtubules regulate their own nucleation. New Journal of Physics, 20. DOI: 10.1088/1367-2630/aac2a5

Kelly AE, Ghenoiu C, Xue JZ, Zierhut C, Kimura H, Funabiki H. (2010). ‘Survivin reads phosphorylated histone H3 threonine 3 to activate the mitotic kinase Aurora B.” Science. 330(6001):235-9. Doi: 10.1126/science.1189505.

Kim H and Stumpff J. (2018). Kif18A promotes Hec1 dephosphorylation to coordinate chromosome alignment with kinetochore microtubule attachment. bioRxiv doi: https://doi.org/10.1101/304147.

Kline-Smith S. L., Khodjakov A., Hergert P. and Walczak C. E. (2004). “Depletion of centromeric MCAK leads to chromosome congression and segregation defects due to improper kinetochore attachments.” Mol. Biol. Cell 15, 1146-1159. DOI: 10.1091/mbc.e03-08-0581.

Krenn V, Musacchio A (2015). The Aurora B kinase in chromosome bi-orientation and spindle checkpoint signaling. Front Oncol 5, 225.

Kucharski, T., hards, R., Godek, K., Gerber, S., Compton, D. (2021) “Chromosome segregation fidelity is controlled by small changes in phosphor occupancy at the kinetochore-microtuble interacte” bioRxiv

Lan, W., Xhang, X., Kline-Smith, S., Rosaco, S., Barret-Wilt, G., Shabanowitz, J., Hunt, D., Walczak, C., Stuckenberg, P. “Aurora B phosphorylates centromeric MDCK and regulates its localization and microtubule depolymerization activity.” Curr Biol. 14(4):273-86. DOI: 10.1016/j.cub.2004.01.055.

Lampson MA, Grishchuk EL. (2017). “Mechanisms to Avoid and Correct Erroneous Kinetochore-Microtubule Attachments.” Biology (Basel). 6(1):1. Doi: 10.3390/biology6010001.

Lee CW, Ferreon JC, Ferreon AC, Arai M, Wright PE. (2010). “Graded enhancement of p53 binding to CREB-binding protein (CBP) by multisite phosphorylation”. Proc Natl Acad Sci 2010;107:19290–19295. Doi: 10.1073/pnas.1013078107

Lerner E, Barth A, Hendrix J, Ambrose B, Birkedal V, Blanchard SC, Börner R, Sung Chung H, Cordes T, Craggs TD, Deniz AA, Diao J, Fei J, Gonzalez RL, Gopich IV, Ha T, Hanke CA, Haran G, Hatzakis NS, Hohng S, Hong SC, Hugel T, Ingargiola A, Joo C, Kapanidis AN, Kim HD, Laurence T, Lee NK, Lee TH, Lemke EA, Margeat E, Michaelis J, Michalet X, Myong S, Nettels D, Peulen TO, Ploetz E, Razvag Y, Robb NC, Schuler B, Soleimaninejad H, Tang C, Vafabakhsh R, Lamb DC, Seidel CA, Weiss S. (2021). “FRET-based dynamic structural biology: Challenges, perspectives and an appeal for open-science practices.” Elife. 2021 10:e60416. DOI: 10.7554/eLife.60416.

Long AF, Kuhn J, Dumont S. The mammalian kinetochore-microtubule interface: robust mechanics and computation with many microtubules. Current Opinion in Cell Biology 60, 60–67 (2019).

Liu D, Vader G, Vromans MJ, Lampson MA, Lens SM. (2009) “Sensing chromosome bi-orientation by spatial separation of aurora B kinase from kinetochore substrates” Science 323:1350–1353. DOI: 10.1126/science.1167000.

Malaby H., Dumas, M., Ohi, R,, and Stumpff, J. (2019). “Kinesin binding protein ensures accurate chromosome segregation by buffering Kif18A and Kif15”. JCB 218: 1218-1234. DOI: 10.1083/jcb.201806195.

Maliga Z, Kapoor TM, Mitchison TJ. (2002). “Evidence that monastrol is an allosteric inhibitor of the mitotic kinesin Eg5.” Chem Biol. 9(9):989-96. Doi: 10.1016/s1074-5521(02)00212-0.

Manning, A., Bakhoum, S., Maffini, S., Correia-Melo, C., Maiato, H., Compton, D. (2010). “CLASP1, Astrin and Kif2b form a molculear switch that regulation kinetochore-microutbule dynamics to promote mitotic progression and fidelity”. EMBO J. 29(20):3531-43. DOI: 0.1038/emboj.2010.230.

Manning AL, Ganem NJ, Bakhoum SF, Wagenbach M, Wordeman L, Compton DA. (2007) “The kinesin-13 proteins Kif2a, Kif2b, and Kif2c/MCAK have distinct roles during mitosis in human cells.” Mol Biol Cell. 18: 2970-9. DOI: 10.1091/Mbc.E07-02-0110

Marquis, C., Fonseca, C., Queen, K., Wood, L., Vandal, S., Malaby, H., Clayton, J., Stumpff, J. (2021). “Chromosomally unstable tumor cells specifically require Kif18A for profileration.” Nat Comm. 12(1213). DOI: 10.1038/s41467-021-21447-2

Mayr M. I., Hümmer S., Bormann J., Grüner T., Adio S., Woehlke G., and Mayer T. U. (2007). “The human kinesin Kif18A is a motile microtubule depolymerase essential for chromosome congression.” Curr. Biol. 17, 488-498. DOI: 10.1016/j.cub.2007.02.036

McAinsh, A., Marston, A. (2022). “The Four Causes: The Functional Architecture of Centromeres and Kinetochores.” Ann Rev Gen. 56, 279-314. DOI: 10.1146/annurev-genet-072820-034559.

McHugh, T., Zou, J., Volkov, V., Bertin, A., Talapatra, S., Rappsilber, J., Dogterom, M., Welburn J. (2019) “The depolymerase activity of MCAK shows a graded response to Aurora B kinase phosphorylation through allosteric regulation.” J Cell Sci 132 (4). DOI: 10.1242/jcs.228353

McIntosh, J. R. (1991). “Structural and mechanical control of mitotic progression.” Cold Spring Harbor Symp. Quant. Biol. 56, 613-619.

McVey SL, Cosby JK, Nannas NJ. (2021) “Aurora B Tension Sensing Mechanisms in the Kinetochore Ensure Accurate Chromosome Segregation.” Int J Mol Sci. 22(16):8818. DOI: 10.3390/ijms22168818.

Mitevska, O., Lam, P., Daly, L., Auckland, O. (2022). “Lis1–dynein drives corona compaction and limits erroneous microtubule attachment at kinetochores “ J Cell Sci. 136(5). DOI: 10.1242/jcs.260226

Monda JK, Cheeseman IM: The kinetochore-microtubule interface at a glance. J Cell Sci 2018, 131.

Musacchio A. and Desai A. (2017). “A molecular view of kinetochore assembly and function. Biology.” 6, 5 DOI: 10.3390/biology6010005

Nezi L, Musacchio A. (2009). “Sister chromatid tension and the spindle assembly checkpoint.” Curr Opin Cell Biol. 21(6):785-95. DOI: 10.1016/j.ceb.2009.09.007.

Nicklas RB, Koch CA. (1969) “Chromosome micromanipulation. 3. Spindle fiber tension and the reorientation of mal-oriented chromosomes” The Journal of Cell Biology. 43:40–50. DOI: 10.1083/jcb.43.1.40

Orr, B., Lama, T., Liu, Z., Kwok, B., Compton D. (2016). “Adaptive resistance to an inhibitor of chromosomal instability in human cancer cells.” Cell Rep. 17(7); 1755-1763. DOI: 10.1016/j.celrep.2016.10.030.

Posch M, Khoudoli GA, Swift S, King EM, Deluca JG, Swedlow JR (2010) Sds22 regulates aurora B activity and microtubule-kinetochore interactions at mitosis The Journal of Cell Biology 191:61–74. DOI: 10.1083/jcb.200912046

Powers A.F., Franck A.D., Asbury C.L. et al. (2009). “The Ndc80 kinetochore complex forms load-bearing attachments to dynamic microtubule tips via biased diffusion.” Cell. 136: 865-875. Doi: 10.1016/j.cell.2008.12.045.

Pufall MA, Lee GM, Nelson ML, Kang HS, Velyvis A, Kay LE, McIntosh LP, Graves BJ. (2005). “Variable control of Ets-1 DNA binding by multiple phosphates in an unstructured region.” Science. 309:142–145. Doi: 10.1126/science.1111915.

Raaijmakers, J., Tanenbaum, M., Maia, A., Medema, R. (2009). “RAMA1 is a novel kinetochore protein involved in kinetochore-microtubule attachment.”
J. Cell Sci., 122, pp. 2436-2445. DOI:

Rendli P.M., Gasic I., Meraldi P., Nigg E.A., Santamaria A. (2016) “The Ska complex promotes Aurora B activity to ensure chromosome biorientation.” J. Cell Biol. 215:77–93. DOI: 10.1083/jcb.201603019.

Rosas-Salvans, M., Sutanto, R., Suresh, P., Dumont, S. (2002). “The Astrin-SKAP complex reduces friction at the kinetochore-microtubule interface” 32(12): pp.2621-2631. DOI: 10.1016/j.cub.2022.04.061

Salimian KJ, Ballister ER, Smoak EM, Wood S, Panchenko T, Lampson MA, Black BE. (2011). “Feedback control in sensing chromosome biorientation by the Aurora B kinase.” Curr Biol. 21(13):1158-65. Doi: 10.1016/j.cub.2011.06.015.

Sarangapani K, Koch L, Nelson C, Asbury C, Biggins S. (2021). “Kinetochore-bound Mps1 regulates kinetochore-microtubule attachments via Ndc80 phosphorylation.” J Cell Biol. 220(12):e202106130. Doi: 10.1083/jcb.202106130.

Schmidt JC, Arthanari H, Boeszoermenyi A, Dashkevich NM, Wilson-Kubalek EM, Monnier N, Markus M, Oberer M, Milligan RA, Bathe M, et al. (2012). “The kinetochore-bound Ska1 complex tracks depolymerizing microtubules and binds to curved protofilaments.” Dev Cell. 23:968–80. DOI:

Schwietert, F., Volkov, V., Veld, P., Dogterom, M., Musacchio, A., Kierfeld, J. (2022). “Strain stiffening of Ndc80 complexes attached to microtubule plus ends.” Biophys J. 121(21):4048-4062. Doi: 10.1016/j.bpj.2022.09.039.

Shao, H., Huang, Y., Zhang, L., Yuan, K., Chu, Y., Dou, Z., Jin, C., Garcia-Barrio, M., Liu, X., Yao, X. (2015). “Spatiotemporal dynamics of Aurora B-PLK1-MCAK signaling axis orchestrates kinetochore bi-orientation and faithful chromosome segregation.” Scientific Reports. 5, 12204. DOI: 0.1038/srep12204.

Skibbens RV, Skeen VP, Salmon ED (1993).” Directional instability of kinetochore motility during chromosome congression and segregation in mitotic newt lung cells: a push-pull mechanism.” J Cell Biol. 122:859–875. DOI: 10.1083/jcb.122.4.859

Silbey, R., Alberty, R., Bawendi, M. Physical Chemistry. Wiley. (2005).

Sivakumar S., Janczyk P., Qu Q., Brautigam C.A., Stukenberg P.T., Yu H., Gorbsky G.J. (2016) The Human SKA Complex Drives the Metaphase-Anaphase Cell Cycle Transition by Recruiting Protein Phosphatase 1 to Kinetochores. Elife. 5:e12902. DOI: 10.7554/eLife.12902.

Steblyanko, Y., Rajendraprasa, G., Osswald, N., Eibes, S., Jacome, A., Geley, S., Pereira, A., Maiatio, H., Barisic, M. (2020). "Microtubule poleward flux in human cells is driven by the coordinated action of four kinesins" *EMBO* 39: 9:e105432 DOI: 10.15252/embj.2020105432

Stumpff, J., Von Dassow, G., Wagenback, M., Asbury, C., Wordeman, L. (2008). "The Kinesin-8 motor, Kif18A, suppresses kinetochore movement to control mitotic chromosome alignment." Dev Cell. 14(2): 252-262. DOI: 10.1016/j.devcel.2007.11.014.

Suzuki, A., Badger, B., Salmon ED. (2015). "A quantitative description of Ndc80 complex linkage to human kinetochores" Nat Comm. 6:8161. DOI: 10.1038/ncomms9161.

Tamayo, N., Bourbeau, M., Allen, J., Ashoton, K., Chen, J., Kaller, M., Nguyen, T., Nishimura, N., Pettus, L., Walton, M., Belmontes, B., Moriguschi, J., Chen, K., McCarter, J., Hanestad, K., Chung, G., Ninniri, M.S., Sun, J., Ppoppe, L., Spahr, C., Hui, J., Jia, L, Wu, T., Dahal, U.,

Tanaka TU, Rachidi N, Janke C, Pereira G, Galova M, Schiebel E, Stark MJ, Nasmyth K. (2002). "Evidence that the Ipl1-Sli15 (Aurora kinase-INCENP) complex promotes chromosome bi-orientation by altering kinetochore-spindle pole connections." Cell. 108(3):317-29. Doi: 10.1016/s0092-8674(02)00633-5.

Tanaka TU, Zhang T. (2022). "SWAP, SWITCH, and STABILIZE: Mechanisms of Kinetochore-Microtubule Error Correction." Cells. 11(9):1462. Doi: 10.3390/cells11091462

Theis, M., Slabicki, M., Junqueira, M., Paszkowski-Rogacz, M., Sontheimer, J., Kittler, R., Heninger, A., Glatter, T., Kruusmaa, K., Poser, I., (2009). "Comparative profiling identifies C13orf3 as a component of the Ska complex required for mammalian cell division." EMBO J., 28 pp. 1453-1465 DOI:

Tauchman EC, Boehm FJ, DeLuca JG. (2015). "Stable kinetochore-microtubule attachment is sufficient to silence the spindle assembly checkpoint in human cells." Nat Comm. 6:10036. Doi: 10.1038/ncomms10036. PMID: 26620470

Wan X, Cimini D, Cameron LA & Salmon ED (2012). "The coupling between sister kinetochore directional instability and oscillations in centromere stretch in metaphase PtK1 cells." Mol. Biol. Cell 23: 1035–1046. DOI: 10.1091/mbc.E11-09-0767

Wang E, Ballister ER, Lampson MA. (2011). "Aurora B dynamics at centromeres create a diffusion-based phosphorylation gradient." J Cell Biol. 194:539–549

Wang F, Dai J, Daum JR, Niedzialkowska E, Banerjee B, Stukenberg PT, Gorbsky GJ, Higgins JM. (2010). "Histone H3 Thr-3 phosphorylation by Haspin positions Aurora B at centromeres in mitosis." Science. 330(6001):231-5. Doi: 10.1126/science.1189435.

Wang F, Ulyanova NP, Daum JR, Patnaik D, Kateneva AV, Gorbsky GJ, Higgins JM .(2012) "Haspin inhibitors reveal centromeric functions of Aurora B in chromosome segregation" The Journal of Cell Biology 199:251–268. DOI: 10.1074/jbc.M110.181545.

Warren, J., Valles, S., Compton, D. (2021) "Kinetochores respond to subtle changes in the stability of microtubule attachemnts." bioRxiv

Welburn JP, Grishchuk EL, Backer CB, Wilson-Kubalek EM, Yates JR, 3rd, Cheeseman IM. (2009). "The human kinetochore Ska1 complex facilitates microtubule depolymerization-coupled motility." Dev Cell. 16:374–85. DOI:

Welburn JP, Vleugel M, Liu D, Yates JR 3rd, Lampson MA, Fukagawa T, Cheeseman IM. (2010). "Aurora B phosphorylates spatially distinct targets to differentially regulate the kinetochore-microtubule interface." Mol Cell. 38(3):383-92.

Wimbish R, DeLuca JG. (2020a). "Hec1/Ndc80 Tail Domain Function at the Kinetochore-Microtubule Interface." Front. Cell Dev. Biol. DOI: 10.3389/fcell.2020.00043.

Wimbish RT, DeLuca KF, Mick JE, Himes J, Jimenez- Sanchez Jeyaprakash AA, DeLuca JG. (2020b). "The Hec1/ Ndc80 tail domain is required for force generation at kinetochores, but is dispensable for kinetochore-microtubule attachment formation and Ska complex recruitment." Mol Biol Cell. DOI: 10.1091/mbc.E20-05-0286

Wordeman L. and Mitchison T. J. (1995). "Identification and partial characterization of mitotic centromere-associated kinesin, a kinesin-related protein that associates with centromeres during mitosis." J. Cell Biol. 128, 95-104. DOI: 10.1083/jcb.128.1.95

Worderman, L., Wagenbach, M., von Dassow, G. (2007). "MCAK facilitates chromosome movement by promotintg kinetochore microtubule turnover." J Cell Biol. 179(5) 869-79. DOI: 10.1083/jcb.200707120.

Wu, H-Y., Nazockdast, E., Shelley, M., Needleman, D. (2016). "Forces positioning the mitotic spindle: Theories, and now experiments." Bioessays. 38(1600212). DOI: 10.1002/bies.201600212.

Yamagishi Y, Honda T, Tanno Y, Watanabe Y. (2010). "Two histone marks establish the inner centromere and chromosome bi-orientation." Science. 330(6001):239-43. Doi: 10.1126/science.1194498

Yu, C-H., Redemann, S., Yu, H-Y., Kiewisz, R,. Yoo, T., Conway, W., Farhadifar, R., Müller-Reichert, T., Needleman, D. „Central-spindle microtubules are strongly coupled to chromosomes during both anaphase A and anaphase B." Mol Biol Cell. 30 pp. 2503-2514. DOI: 10.1091/mbc.E19-01-0074.

Zaytsev, A., Mick, J., Maslennikov, E., Nikashin, B.,. DeLuca, J., Grishchuk, E. (2015). "Multisite phosphorylation of the NDC80 complex gradually tunes its microtubule-binding affinity" Mol Biol Cell. 15; 26(10): 1829–1844. Doi: 10.1091/mbc.E14-11-1539

Zaytsev AV, Segura-Peña D, Godzi M, Calderon A, Ballister ER, Stamatov R, Mayo AM, Peterson L, Black BE, Ataullakhanov FI, Lampson MA, Grishchuk EL (2016) "Bistability of a coupled Aurora B kinase-phosphatase system in cell division" eLife 5:e10644. DOI: 10.7554/eLife.10644.

Zhang X., Lan, W., Ems-McClung, S., Stukenberg, P.T., Walczak, C.E. (2007). "Aurora B phosphorylates multiple sites on mitotic centreomere associated kinesin to spatially and temporally regulate its function." Mol Biol Cell. 18(9):3264-76. DOI: 10.1091/mbc. e07-01-0086.

Zhou J, Yao J, Joshi HC. (2002). "Attachment and tension in the spindle assembly checkpoint." J Cell Sci.;115(Pt 18):3547-55. doi: 10.1242/jcs.00029